

## Cold spray additive manufacturing and repair: Fundamentals and applications



Shuo Yin<sup>a,\*</sup>, Pasquale Cavaliere<sup>b</sup>, Barry Aldwell<sup>a</sup>, Richard Jenkins<sup>a</sup>, Hanlin Liao<sup>c</sup>, Wenya Li<sup>d</sup>, Rocco Lupoi<sup>a,\*</sup>

<sup>a</sup> Trinity College Dublin, the University of Dublin, Department of Mechanical and Manufacturing Engineering, Parsons Building, Dublin 2, Ireland

<sup>b</sup> Department of Innovation Engineering, University of Salento, Via per Arnesano, 73100, Lecce, Italy

<sup>c</sup> ICB UMR 6303, CNRS, Univ. Bourgogne Franche-Comté, UTBM, Belfort, 90010, France

<sup>d</sup> State Key Laboratory of Solidification Processing, Shaanxi Key Laboratory of Friction Welding Technologies, School of Materials Science and Engineering, Northwestern Polytechnical University, Xi'an, PR China

### ARTICLE INFO

#### Keywords:

Additive manufacturing  
Cold spray  
Restoration  
Repair  
Manufacturing strategy  
Machining

### ABSTRACT

Cold spray is a solid-state coating deposition technology which has recently been applied as an additive manufacturing process to fabricate individual components and to repair damaged components. In comparison with fusion-based high-temperature additive manufacturing processes, cold spray additive manufacturing (CSAM) has been shown to retain the original properties of the feedstock, to produce oxide-free deposits, and to not adversely influence underlying substrate materials during manufacture. Therefore, CSAM is attracting considerable attention from both scientific and industrial communities. Although CSAM is an emerging additive manufacturing technology, a body of work has been carried out by various research groups and the technology has been applied across a range of manufacturing areas. The purpose of this paper is to systematically summarize and review the CSAM-related work to date.

## 1. Introduction

### 1.1. Cold spray process principle

Cold spray is a solid-state material deposition process, which was originally developed as a coating technology in the 1980s [1,2]. In this process, high-temperature compressed gases (typically nitrogen, air, or helium) are used as the propulsive gas to accelerate powder feedstock (typically metals and metal matrix composites) to a high velocity (typically higher than 300 m/s), and to induce deposition when the powders impact onto a substrate (typically metals). In contrast to conventional high-temperature deposition processes, the formation of a cold spray deposit relies largely on the particle kinetic energy prior to impact rather than the thermal energy. The feedstock used for cold spray remains solid state during the entire deposition process. Deposition is achieved through local metallurgical bonding and mechanical interlocking which are caused by localized plastic deformation at the inter-particle and particle-substrate interfaces. This allows for the avoidance of defects commonly encountered in high-temperature deposition processes, such as oxidation, residual thermal stress and phase transformation [3–5].

Successful deposition of a cold sprayed deposit requires the feedstock particles to exceed a critical impact velocity [6–13]. In cold spray, the formation of a deposit consists of two different stages. The first stage involves the deposition of an initial layer of particles where bonding occurs between feedstock particles and the substrate material; the second stage is the deposition on top of the layer(s) previously deposited, where bonding occurs between feedstock particles. Each stage has a respective critical velocity, i.e. for particle/substrate bonding and for deposit growth. Particle impact velocity must satisfy both criterions for successful deposition. In general, a higher particle velocity will result in improved deposit quality. Note that when the powder and substrate are the same material, the critical velocity can be considered as the same for both stages. Fig. 1 shows an in-situ observation of a 45 μm aluminium particle impacting onto an aluminium substrate at different velocities, where particle deposition only occurs when the impact velocity is beyond the critical velocity [6]. Critical velocity is not a constant but depends on several factors including material type, particle size, and particle temperature. Larger particles or higher particle temperature upon impact helps to reduce critical velocity [6,10,12–15].

Feedstock for cold spray is typically gas-atomized spherical metal

\* Corresponding authors.

E-mail addresses: [yins@tcd.ie](mailto:yins@tcd.ie) (S. Yin), [lupoir@tcd.ie](mailto:lupoir@tcd.ie) (R. Lupoi).

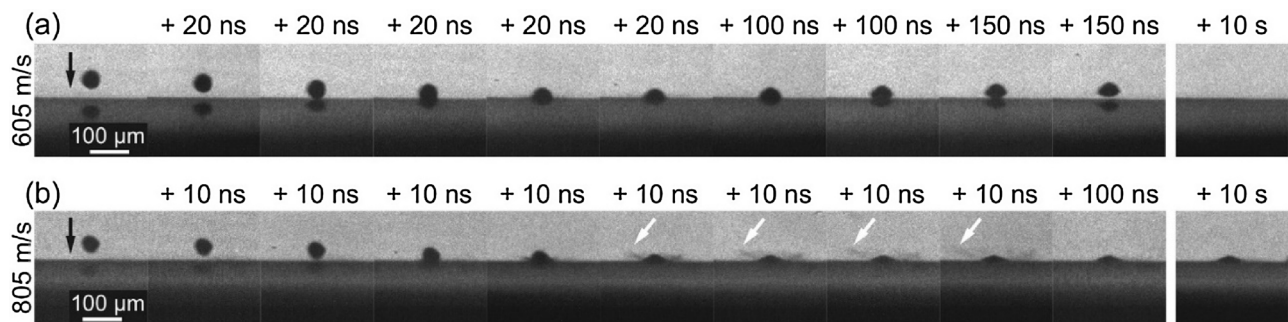


**Fig. 1.** In-situ observation of a 45  $\mu\text{m}$  aluminium particle impacting onto an aluminium substrate at the velocity of (a) 605 m/s and (b) 805 m/s [6]. The critical velocity is between 605 and 805 m/s.

powders, and in some cases irregular powders [5]. The powder size must fall into a specific range, normally between 10 and 100  $\mu\text{m}$  in diameter, to guarantee a sufficiently high particle impact velocity that is beyond the critical velocity [11]. Particles with diameters greater than 100  $\mu\text{m}$  or lower than 10  $\mu\text{m}$  are difficult to accelerate with the propulsive gas and thus usually fail to deposit [16]. For most metals, the most frequently used size-range is 20–60  $\mu\text{m}$ ; for low-density metals such as aluminium and zinc, the upper limit of the size-range can reach 100  $\mu\text{m}$  [11].

### 1.2. Cold spray system nomenclature

The cold spray process can be divided into two categories, according to the pressure of the propulsive gas: high pressure cold spray ( $> 1 \text{ MPa}$ ), and low pressure cold spray ( $< 1 \text{ MPa}$ ). Fig. 2a shows a schematic of a high pressure cold spray system. Compressed gas is divided into two streams upon entering the cold spray system. One stream of the compressed gas (referred to as the propulsive gas) passes through a gas heater, where it is heated to a high temperature. At the same time, the second stream of the compressed gas (referred to as the carrier gas) passes through a powder feeder, where it becomes laden with the

feedstock particles. These two gas streams are then mixed, before entering a de-Laval nozzle, where the gas expands to generate a supersonic gas and powder stream. In order to make certain there is successful injection of the powder into the mixed gas stream the carrier gas pressure must be slightly higher than the propulsive gas pressure. These high-velocity particles impact onto a substrate to form a coating or thick deposit at a temperature well below their melting temperature. Generally, high pressure cold spray systems can operate at the same pressures as low pressure cold spray systems, but the reverse is not true due to the special design of low pressure cold spray systems. Fig. 2b shows a schematic of a low pressure cold spray system. Two obvious differences in the low pressure system from the high pressure system are: the low-pressure compressed gas is normally replaced by a portable air compressor; the powder injection point is at the nozzle divergent section where the local gas pressure is sufficiently low to allow the release of powders from the powder feeder at the atmospheric pressure. These differences make low pressure cold spray systems more flexible and much cheaper in both equipment and processing costs than a high pressure cold spray system [3,5]. They are particularly suitable for the restoration of damaged components due to the portability of the simpler low pressure cold spray systems [17,18]. However, as the particle

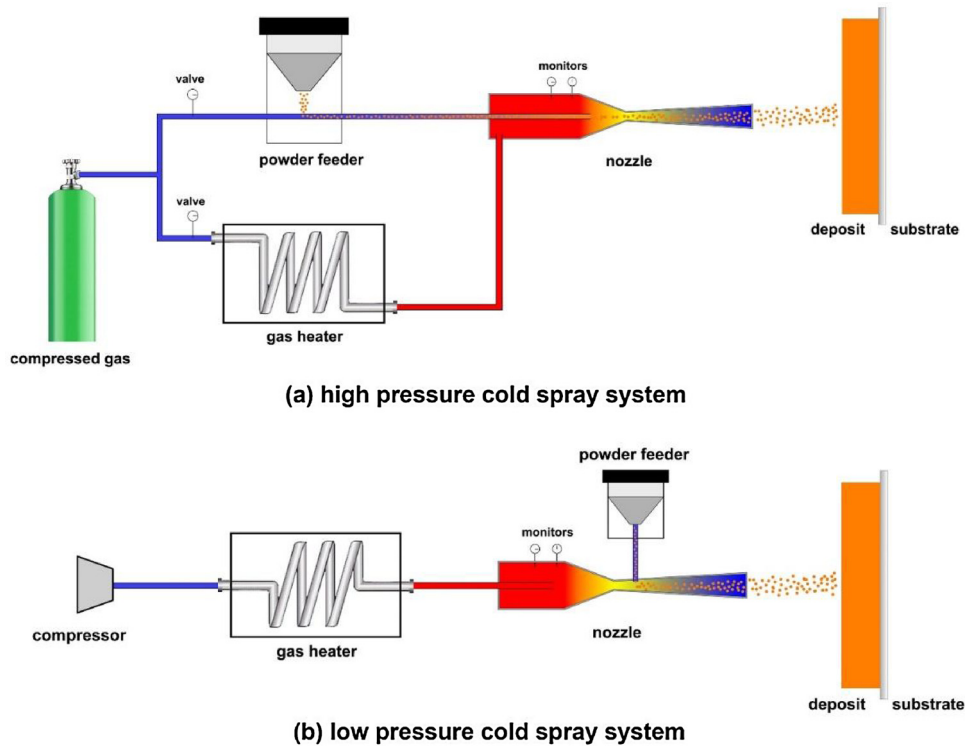


**Fig. 2.** Schematic of high pressure and low pressure cold spray systems.

velocity in low pressure cold spray systems is much lower than in high pressure cold spray systems, the application of low pressure cold spray is significantly limited and only a limited range of materials such as copper and aluminium can be deposited using a low pressure cold spray system. Therefore, in most cases, the term ‘cold spray’ refers to ‘high pressure cold spray’, while ‘low pressure cold spray’ must be specified. This review paper follows this nomenclature.

### 1.3. Cold spray additive manufacturing

Cold spray has been widely applied as a coating technology in a broad range of industries, including aerospace, automotive, energy, medical, marine and other fields. Cold sprayed deposits provide effective protection against high temperature, corrosion, erosion, oxidation and chemicals [19–21]. In recent years, cold spray has been successfully developed as an additive manufacturing technology to fabricate free-standing metal components, and to restore damaged metal components [4,22,23]. This development shines a new light on conventional additive manufacturing technologies, and significantly broadens the applications of cold spray.

As a new member of the additive manufacturing family, cold spray additive manufacturing (CSAM) has all the benefits of cold spray technology. In comparison with other well-investigated fusion-based additive manufacturing technologies such as laser beam melting (LBM), electron beam melting (EBM) and laser metal deposition (LMD) [24,25], CSAM has unique advantages. Table 1 compares the advantages and disadvantages of CSAM and other existing additive manufacturing technologies. As can be seen, the most important benefits of CSAM over other additive manufacturing processes are shorter production times, unlimited product size, high flexibility, and suitability for damaged component repair. Furthermore, CSAM is particularly suitable for high-reflectivity metals such as copper and aluminium, which are very challenging to manufacture using laser based additive manufacturing processes. However, the disadvantages of CSAM are also obvious. CSAM typically fabricates a semi-finished product with a rough surface, which requires post-machining. In addition, CSAM deposits possess poorer mechanical properties in their as-fabricated state due to the inherent defects. As a result, heat treatments are commonly applied to improve the mechanical properties.

Currently, CSAM has been primarily used for fabricating components with rotational symmetry such as cylinder walls, tubes and flanges. With the aid of a well-designed mandrel, spindle, or mask, it is also applicable for the fabrication of complex structures such as array fin heat exchangers, metal labels and metal 2D codes [19]. CSAM is also widely used to repair damaged components due to its high flexibility, lack of adverse effects on the underlying substrate material, and to retain the original properties of the feedstock. So far, CSAM has been successfully applied to restore a variety of corroded and mechanically

damaged components in various fields, particularly in the aerospace industry. Repair using CSAM returns the components to serviceable condition, significantly reducing the cost when compared to replacement with a new component [26]. In recent years, investigations and applications regarding CSAM have been widely reported, although it is still an emerging technology. A systematic summarization on the CSAM-related work is still lacking. Therefore, a review on this topic is urgently needed. This paper aims to provide a comprehensive review of the existing CSAM-related work in the present paper, helping the reader to understand the newly developed CSAM technology.

## 2. Manufacturing parameters for CSAM

In CSAM, the propulsive gas, powder feeder and nozzle must work in unison and under careful control to produce high-quality deposits. Fig. 3 shows a schematic of the typical manufacturing parameters used in CSAM. Manufacturing parameters including the propulsive gas parameters (pressure, temperature and type), powder feeder parameters (powder feed rate), and nozzle parameters (traverse speed, scanning step, standoff distance, spray angle and trajectory) all significantly influence the deposition process, and therefore the deposit quality. Table 2 summarizes some typical deposit properties and their relationship with the manufacturing parameters. Understanding these parameters helps the development of the best CSAM manufacturing strategy and products.

### 2.1. Propulsive gas parameters for CSAM

Propulsive gas parameters are the most important manufacturing parameters in CSAM, as they directly determine particle impact velocity and therefore the properties of the deposit. In general, gases used in CSAM include helium, nitrogen and air. The gas pressure and temperature normally range from 0.5 to 6.0 MPa and from 25 to 1000 °C, respectively. It is well understood that higher gas pressure, higher gas temperature or lower gas molecular weight causes higher particle impact velocity, as can be seen in Fig. 4 [16,27]. Using helium instead of nitrogen and air is the most effective way to increase particle velocity, but the gas cost of helium is also much higher. Otherwise, increasing gas temperature is more effective than increasing gas pressure [16].

To date, it has been widely accepted by the cold spray community that higher particle impact velocity can result in improved deposit properties. As summarized in the Ref [3,5], a large number of experimental works demonstrate that increasing particle impact velocity significantly improves deposition efficiency, deposit porosity, deposit strength (cohesion strength or tensile strength) and adhesion strength due to the reduced inherent defects and enhanced metallic bonding. Fig. 5 shows the effect of particle impact velocity (or propulsive gas parameters) on the deposition efficiency, deposit porosity, deposit

**Table 1**  
Comparison of advantages and disadvantages between CSAM and other fusion-based additive manufacturing.

	CSAM	SLM	EBM	LMD
Powder feed mode	Direct deposition	Powder bed	Powder bed	Direct deposition
Feedstock limitations	Difficulty processing high hardness and strength metals	Difficulty processing high reflectivity and poor flowability metals	Unsuitable for non-conductive and low melting-temperature metals	Difficulty with high reflectivity metals
Powder melting	No	Yes	Yes	Yes
Product size	Large	Limited	Limited	Large
Dimensional accuracy	Low	High	High	Medium
Mechanical properties (AF)	Low	High	High	High
Mechanical properties (HT)	High	High	High	High
Production time	Short	Long	Long	Long
Equipment flexibility	High	Low	Low	Low
Suitable for repair	Yes	No	No	Yes

AF: as-fabricated, HT: heat treatment.

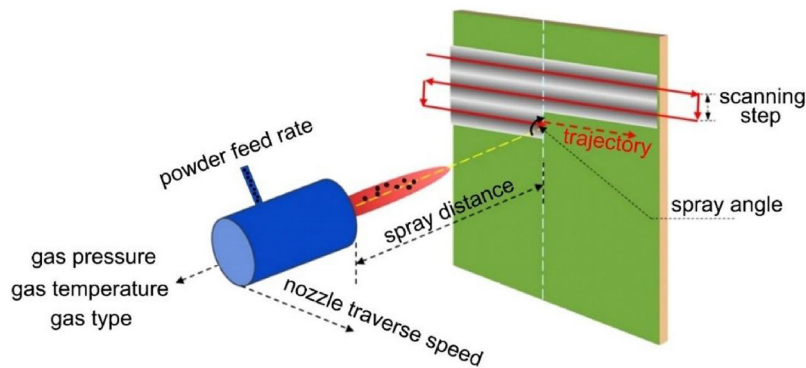


Fig. 3. Schematic of the typical manufacturing parameters used in CSAM.

Table 2

Typical deposit properties affected by the manufacturing parameters.

	Porosity	Deposit strength	Adhesion	Residual stress	Deposition efficiency
Gas pressure ↑	↓	↑	↑	↑	↑
Gas temperature ↑	↓	↑	↑	↑	↑
Gas molecular weight ↑	↑	↓	↓	↓	↓
Powder feed rate ↑	↑	↓	↓	↑	↓
Traverse speed ↑	↑	↑	↑	↓	↑
Scanning step ×	×	×	×	×	×
Standoff distance O	O	O	O	O	O
Spray angle ↑	↓	↑	↑	↑	↑
Trajectory ×	×	×	×	×	×

'↑' increase, '↓' decrease, 'O' relevant but no common view, '×' no data available.

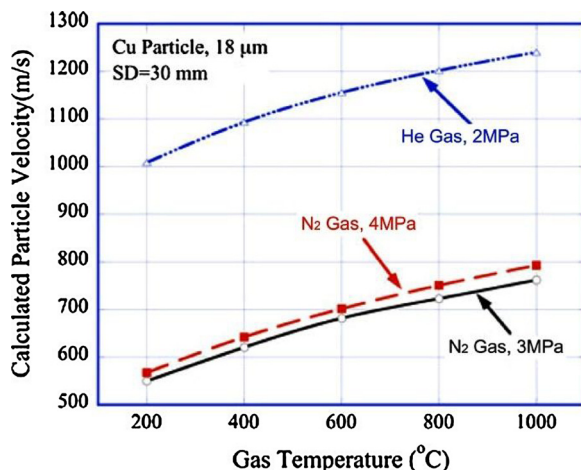


Fig. 4. Modeling result of the particle velocity at the location 30 mm away from the nozzle exit as a function of propulsive gas pressure, temperature, and type [16,27].

strength and deposit adhesion strength of CSAM titanium deposits [28–30]. Due to the enhanced work-hardening effect, increasing the particle impact velocity will increase the deposit hardness. In addition, studies also suggest that higher impact velocity results in higher residual stress in the CSAM deposit due to increased plastic deformation of the particles [31–34]. However, a higher gas temperature was found to relieve the residual stress due to the in-situ annealing effect, therefore meaning that increasing the gas temperature did not significantly increase the residual stresses [35–37].

## 2.2. Powder feeder parameters for CSAM

Powder feed rate is the only parameter controlled by powder feeder. It is defined as the quantity of powder introduced into the nozzle per unit of time. Powder feed rate influences the properties of CSAM deposits in three ways. Firstly, powder feed rate significantly affects the flow stream passing through the nozzle and thus the particle velocity [38–41]. Fig. 6 shows the particle velocity at the nozzle exit as a function of powder mass feed rate [39]. Due to the strong gas-particle interaction at high powder load, particle velocity decreases as the powder feed rate increases. This results in a slight increase in deposit porosity and reduction in deposition efficiency, hardness and tensile strength at increased powder feed rates. However, it should be noted that powder feed rates used in CSAM are typically much lower than 100 g/s, with rates between 10 g/s and 30 g/s being typical. Within this range, the influence of powder feed rate on the particle velocity is not significant [40]. Secondly, powder feed rate also affects the thickness and profile of the single-track deposit; higher powder feed rates result in thicker deposits and sharper track profiles [42,43]. In this regard, powder feed rate has a similar effect as nozzle traverse speed. These two parameters must be considered together when determining the profile of a single-track deposit. A detailed description of the effect of these two parameters on the profile of a single-track will be provided in section 2.3.1. Thirdly, high feed rates can lead to high localized residual stress between deposits and substrate. High residual stresses can cause the delamination of the deposit from the substrate during spraying [40,41], which should be avoided in CSAM. In summary, the three ways in which powder feed rate affects the deposit properties suggest that powder feed rate should not be too high during the CSAM process.

## 2.3. Nozzle parameters for CSAM

### 2.3.1. Nozzle traverse speed

Nozzle traverse speed determines the spray duration and amount of feedstock powder impacting onto the target surface per unit time, thereby directly affecting the deposit thickness and cross-sectional profile of a single-track deposit [40,42–48]. In general, a lower nozzle traverse speed results in a thicker single-layer deposit and sharper cross-sectional profile, as shown in Fig. 7. This can also be achieved through a higher powder feed rate, as addressed in section 2.2 [42,43]. The variation in peak track thickness due to changing nozzle traverse speed is due to different amount of the feedstock powder released per unit time and per unit area; lower nozzle traverse speed and higher powder feed rate can both result in the release of a greater amount of powder per unit time and per unit area. The change in track profile is caused by the flow characteristics of the propulsive gas as it passes through a supersonic nozzle. According to the fluid dynamics theory, particle velocity and the resultant deposition efficiency at the central zone will be higher than at the outer zone [49–51]. Due to this radial variation in velocity the deposit cross-sectional profile will be a

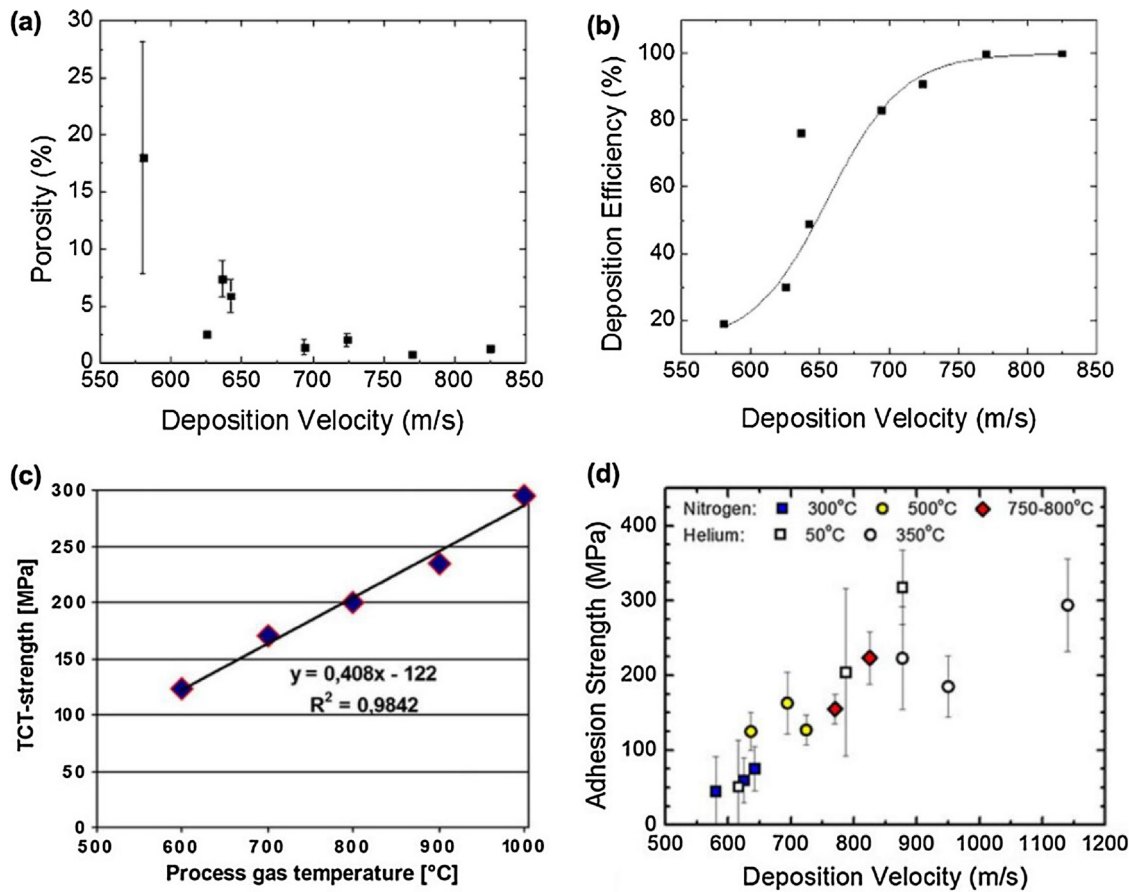


**Fig. 5.** Effect of particle impact velocity (or propulsive gas parameters) on the deposit porosity, deposition efficiency, deposit strength and deposit adhesion strength of CSAM titanium deposits. (a, b) titanium deposits on mild steel substrate at 2–4 MPa and 300–800 °C with nitrogen [28], (c) titanium deposits on an aluminium substrate at 4 MPa with nitrogen [29], and (d) titanium deposits on a titanium substrate at 1–4 MPa with nitrogen and helium [30].

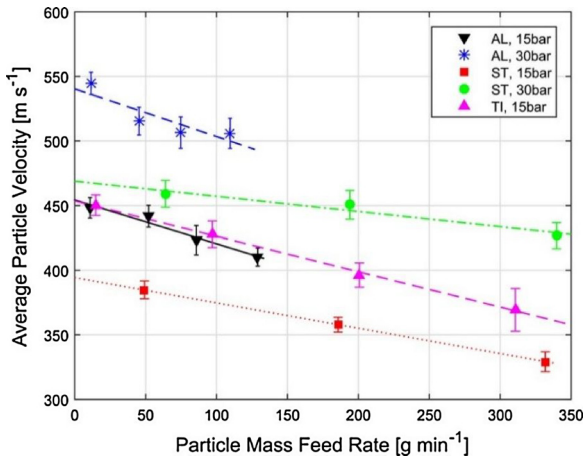


**Fig. 6.** Particle velocity at the nozzle exit as a function of powder mass feed rate [39].

gaussian shape, as shown in Fig. 7. The sloped side of the track introduces an angle to the incident particles of any subsequent layers deposited on top of the track, further decreasing the deposition efficiency of the particles and leading to a much steeper sloped side [42,43]. Therefore, the deposit profile becomes increasingly steeper as the nozzle traverse speed decreases and the powder feed rate increases. In real world applications of CSAM, the control of the thickness and profile of a single-track deposit is realized by coordination of the nozzle traverse speed and powder feed rate [42,43].

Nozzle traverse speed also significantly influences the deposit microstructure and properties. The deposit density increases as the nozzle traverse speed decreases, but there is also a reduction in the mechanical properties of the deposit, such as elastic modulus, deposit strength, and adhesion strength with the substrate [47,52,53]. Fig. 8 shows cross-sectional images of Ti6Al4V deposited onto Ti6Al4V substrates using different nozzle traverse speeds [47]. It can be clearly seen that the porosity increases as the nozzle traverse speed increases. Moreover, at the lowest speed shown in Fig. 8a, delamination of the deposit from the substrate is observed, suggesting low adhesion strength caused by high residual stresses [40,47]. Delamination at low nozzle traverse speeds and high powder feed rates was also reported in other studies, and frequently occurred in the authors' experiments [40]. Another potential effect of nozzle traverse speed is heating of the deposit and/or substrate by the high-temperature impinging jet. Lower traverse gun speed results in higher deposit and substrate temperatures, which contributes to the deposition process [47,54] but in turn causes thermal stresses at the interface [55].

Currently, there are no general rules on how to select the nozzle traverse speed. However, according to existing studies and the experience of the authors', the use of low nozzle traverse speeds often results in high localized residual stresses between the deposit and substrate, and low adhesion strength. These are undesirable for the application of CSAM for the repair of damaged components [40]. Therefore, it is not recommended to use a low nozzle traverse speed for CSAM.

### 2.3.2. Nozzle scanning step

The build-up of a CSAM deposit is achieved through nozzle scanning over the entire target surface line by line and layer by layer according to

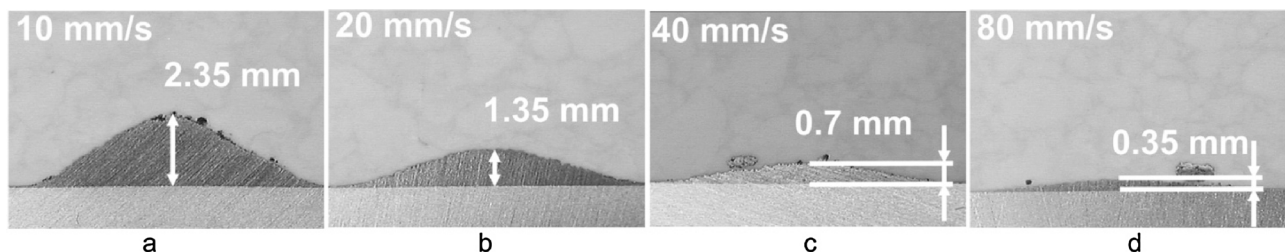


**Fig. 7.** Effect of nozzle traverse speed on the single-track deposit thickness and cross-sectional profile [46].

a pre-defined trajectory. In other words, the deposit is produced through the stacking of many single-track deposits. The most frequently used scanning strategy is an overlapping strategy where two neighbouring single-tracks overlap each other, as shown in Fig. 9. The scanning step is then defined as the interval between the centerlines of two single-track deposits. The main influence of scanning step on the deposit is the on the uniformity of the deposit thickness and the surface morphology; a properly chosen scanning step will lead to a homogeneous deposit and smooth surface.

The selection of scanning step depends upon the width of a single-track deposit. In the authors' experiments, the scanning step is always defined as half of the single-track width to guarantee the flatness of the deposit surface. However, a recent study has demonstrated that a more deliberate selection of scanning step can result in a less undulating surface. In that study, the optimum scanning step was estimated by using a self-developed software, Toolkit, [56]. Fig. 10 shows the deposit thickness of cold sprayed aluminium as predicted by Toolkit and as measured experimentally, for two values of scanning step. Clearly, under the optimum scanning step (4 m m), the deposit thickness is more consistent than when using a larger scanning step (7 m m). This clearly shows the importance of scanning step in CSAM. However, investigations on the effects of varying scanning step are quite rare. The effect, if any, of scanning step on the deposit properties is not understood. Relevant studies are urgently needed on this topic.

### 2.3.3. Standoff distance

Standoff distance is defined as the distance between nozzle outlet and the target surface. In a supersonic free jet, the intensity of the jet core decreases gradually along the jet central axis due to momentum exchange between the jet and the atmosphere [51,57]. Inside the jet core, particles are subject to positive drag forces and thus rapidly accelerate. However, a short distance after the gas exits the diverging section of the nozzle, the gas decelerates to lower than the particle velocity and the resultant negative drag force causes the deceleration of particles. As a result, the particle impact velocity and deposition efficiency increase as the standoff distance increases from zero, but then reduces after an optimal operating point [58]. This phenomenon has been experimentally confirmed in CSAM aluminium, copper and titanium deposits in the work of Pattison et al. [58] and copper deposits in

the work of Li et al., as shown in Fig. 11 [59]. However, Li et al. reported a much shorter optimal standoff distance, and also a monotonic reduction of deposition efficiency in aluminium and titanium deposits as the standoff distance increased from 10 mm to 110 mm. Besides these two investigations, there are also other studies focusing on the effect of standoff distance [60–63], but a consensus on the effect of nozzle standoff distance in CSAM cannot be drawn due to the small number of studies. Although most of the existing work used 10–40 mm as the standoff distance for manufacturing, the effect of standoff distance on the CSAM deposit properties is not well understood. Even for the most thoroughly investigated parameter, deposition efficiency, there is no consistent conclusion to date. Therefore, more investigation on this topic is required to fully clarify the effect of standoff distance on CSAM.

### 2.3.4. Spray angle

Spray angle is defined as the angle of the nozzle central axis to the target surface. It has a significant influence on the vector components of particle impact velocity, and consequently on the deposit properties. When spraying at an angle other than normal to the substrate surface, only the normal velocity component contributes to the particle deposition, while the tangential velocity component can play an opposing role by potentially detaching the deposited particles [64,65]. As the spray angle decreases, the normal velocity component reduces but the tangential velocity component increases, which significantly deteriorates the deposit quality. Deposition efficiency, deposit strength and adhesion strength all reduce with decreasing spray angle [29,60,66–70]. This can be clearly noticed from Fig. 12 showing the increasing porosity in a titanium deposit with reducing spray angle [29]. In addition, modelling work has suggested that residual stresses decrease as the spray angle is reduced, but there is no experimental validation available so far [32].

Spray angle also affects the cross-sectional profile of single-track deposits. The profile of a track sprayed at an angle will have a skewed shape, as shown in Fig. 13. This is due to the inclined nozzle causing inconsistent standoff distance and thus non-uniform deposition efficiency over the particle impact area [48]. This may result in inhomogeneity of the deposit. Overall, angular spraying is harmful to the overall deposit performance; hence spraying at angles other than normal to the substrate has to be avoided in CSAM.

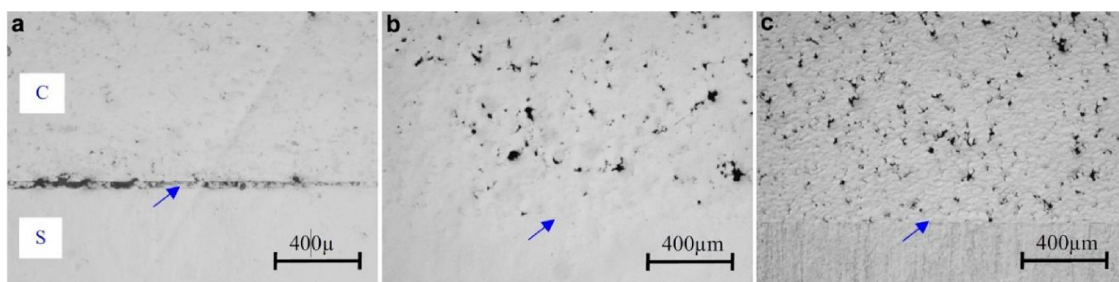


**Fig. 8.** Cross-sectional image of Ti6Al4V deposits onto Ti6Al4V substrates fabricated under different nozzle traverse speed. (a) 100 mm/s, (b) 300 mm/s and (c) 500 mm/s. Blue arrows indicate the deposit-substrate interface [47](For interpretation of the references to colour in this figure legend, the reader is referred to the web version of this article).

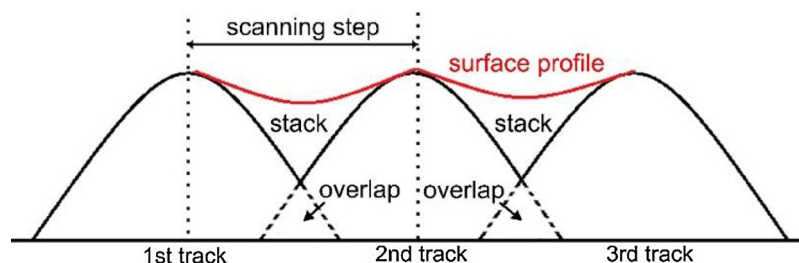
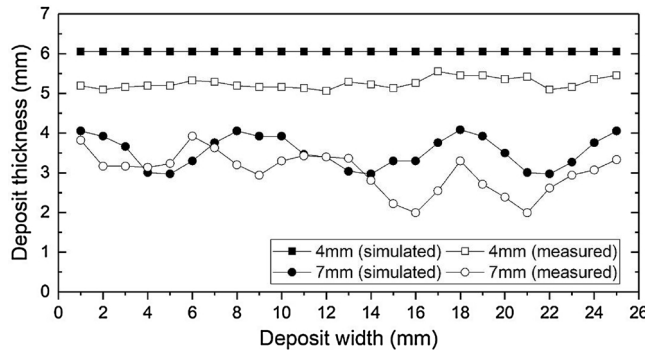


Fig. 9. Schematic of scanning step definition.



**Fig. 10.** Simulated surface flatness of aluminium deposit by Toolkit and measured one under the scanning steps of 4 mm and 7 mm. The width of the single-track is 16 mm. Data was picked from Ref [56] and replotted.

### 2.3.5. Nozzle trajectory

Nozzle trajectory is defined as the path that nozzle takes during the manufacturing process. The basic principle of trajectory definition is to ensure homogeneous density and properties of the deposit. In general, when spraying on a flat surface, a simple round-trip (also known as a zig-zag pattern) trajectory is always applied. This trajectory is easy to define and able to yield a homogeneous deposit [52]. However, for a complex curved surface, trajectory definition should ensure that the standoff distance, spray angle, nozzle speed and other manufacturing parameters are kept constant over the curved surface to avoid any inhomogeneity of the deposited material. In addition, trajectory definition should also consider the curvature and transition between different features [71]. Nozzle trajectories for complex surfaces are normally defined on an off-line programming platform by the aid of CAD/CAM software to accurately control the nozzle parameters and to adapt them to the surface topography [23]. Fig. 14 shows a nozzle trajectory definition for depositing a turbine blade surface, and the resultant cold

sprayed MCrAlY coating [72,73]. The trajectory was first programmed on an off-line platform to define the nozzle traverse speed, scanning step, standoff distance and spray angle as shown in Fig. 14a. This trajectory was then executed by a robot arm, with the as-sprayed coating shown in Fig. 14b.

A recent study reported a novel spiral trajectory for the restoration of damaged aluminium coupons using CSAM. Fig. 15 shows this spiral trajectory and a repaired coupon [74]. This strategy included varying the nozzle traverse speed in inverse proportion to the crater depth, to produce a homogenous deposit and to save feedstock. The nozzle traverse speed at the central area was set lower than the surrounding area, as shown in Fig. 15a. This will create a thicker deposit in the central deep area than in the surrounding shallow area, and thus the final repaired surface will be flat. The repaired coupon is shown in Fig. 15b, and clearly shows the advantages of this trajectory. The repaired surface is very flat without any significant redundant material in the deposit. However, this trajectory may also bring some negative impacts, as varied nozzle traverse speed will result in a nonhomogeneous microstructure and properties in the deposit as addressed in section 2.3.1. To date investigations on nozzle trajectory have been very limited. More investigations on the trajectory development and use of novel trajectory strategies are strongly encouraged.

## 3. Properties of CSAM deposits

Many studies have been carried out to investigate the properties of CSAM deposits. In general, as-fabricated CSAM deposits contain compressive residual stress which are caused by the accumulation of peening stress between successive deposited layers [31,75]; such compressive residual stress in the deposits can be released through post-spray annealing [76,77]. Additionally, CSAM deposits normally have worse mechanical properties in their as-fabricated state, such as lower ductility, lower electrical conductivity, and lower thermal conductivity when compared to bulk materials or fusion-based additive

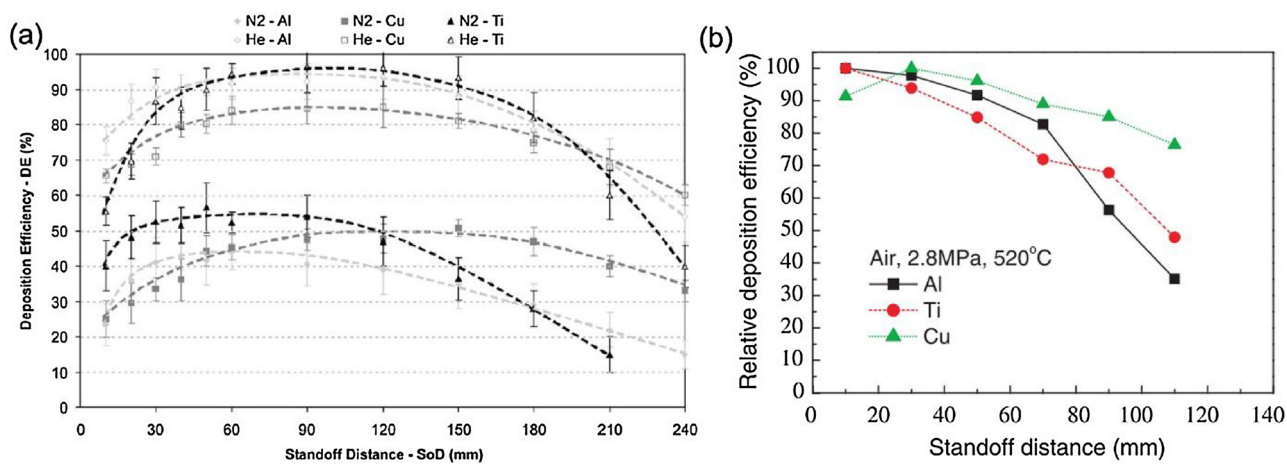


**Fig. 11.** Deposition efficiency as a function of standoff distance (a) Ref [58] and (b) Ref [59].

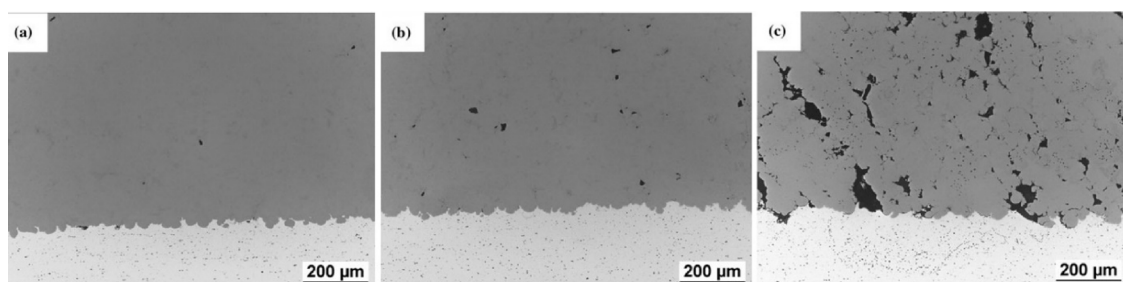


Fig. 12. Cross-sectional images of CSAM titanium deposit produced under the spray angle of (a) 90°, (b) 75° and (c) 45° [29].

manufactured materials. This is due to the inherent defects found in cold sprayed deposits [78]. With suitable heat treatments, the mechanical properties can be significantly improved, to similar levels as bulk materials. In this section, the general properties of CSAM deposits before and after heat treatment are summarized and reviewed. As one of the most frequently used CSAM materials, copper is used as an example throughout.

### 3.1. Defects of CSAM deposits

Deposit defects such as micro-pores and inter-particle boundaries are commonly found in CSAM deposits. These defects are caused by insufficient particle plastic deformation and poor inter-particle bonding during deposition. These defects generally exist in the as-fabricated CSAM deposits, particularly when the particle impact velocity is low. As structural weaknesses, defects have a significant negative impact on the mechanical properties of the deposit. For CSAM copper deposits, micro-

pores are seldom found in the deposit, even under low particle impact velocity, due to the excellent ductility and low strength to density ratio of copper [79]. Thus, for copper the dominant defect that reduces the mechanical properties is the inter-particle boundaries. However, for other materials such as steel [80] or titanium [28], micro-pores are frequently found in the deposits due to their high hardness or high strength to density ratio. In these cases, both micro-pores and inter-particle boundaries affect the deposit properties. Many studies have demonstrated that the detrimental effect of micro-pores and inter-particle boundaries can be reduced by increasing particle impact velocity to enhance particle plastic deformation, or by post-heat-treatment to induce recrystallization within deposited particles and across the inter-particle boundaries [81–92].

Increasing particle impact velocity is the most straightforward way to reduce micro-pores and improve inter-particle bonding in CSAM deposits [8,14,83]. Particle deformation increases at higher impact velocities, preventing the formation of micro-pores [14]. Additionally,

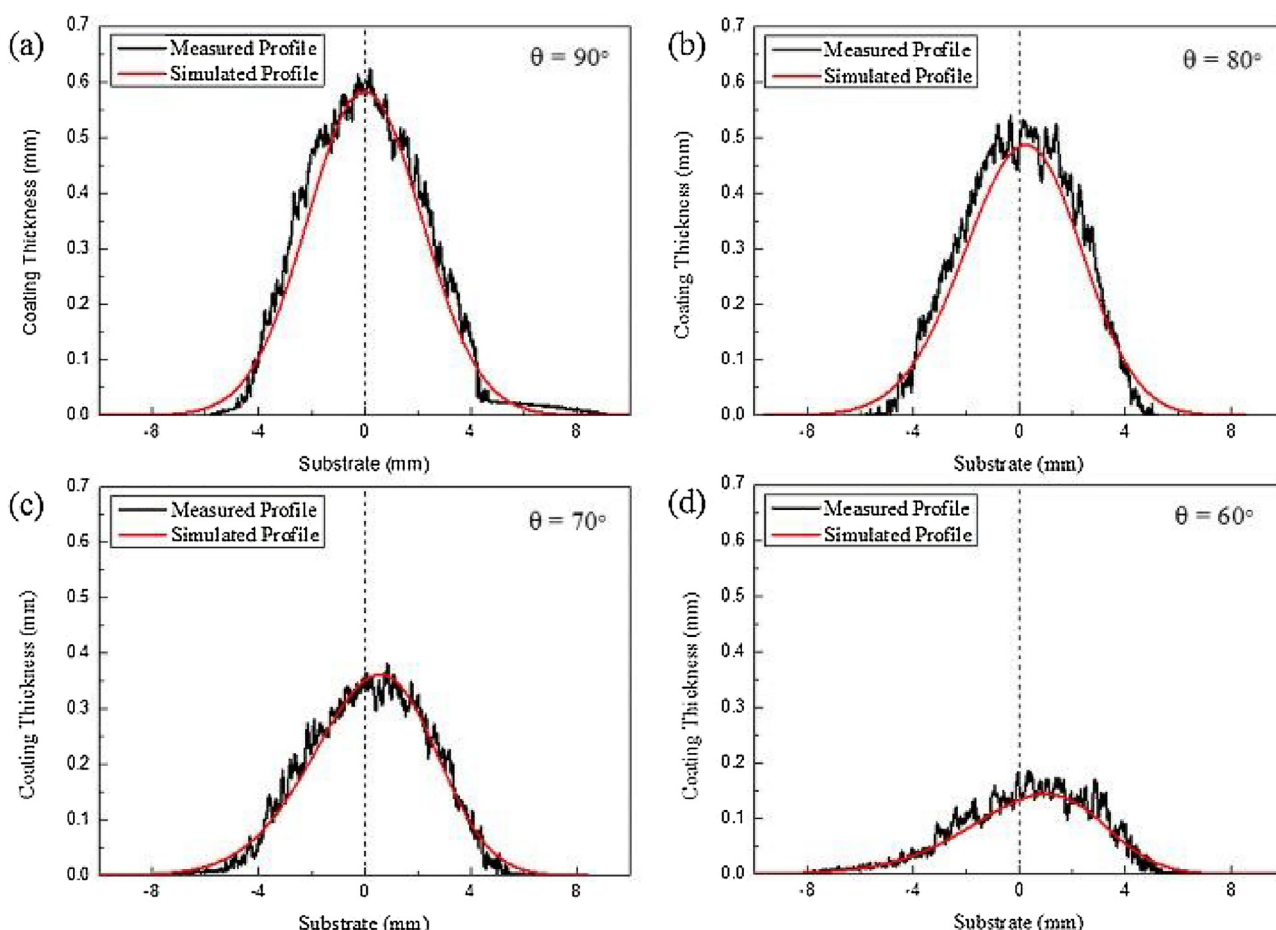


Fig. 13. Effect of spray angle on the single-track deposit cross-sectional profile [48].

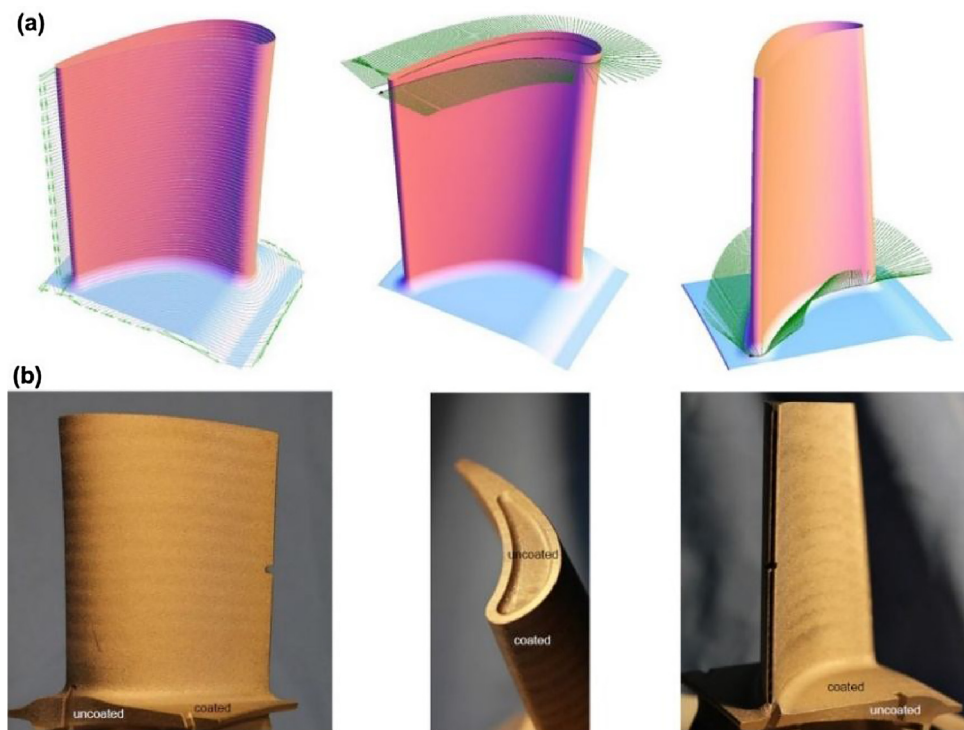


Fig. 14. (a) Nozzle trajectory for depositing a turbine blade surface and (b) the resultant cold sprayed MCrAlY coating [72,73].

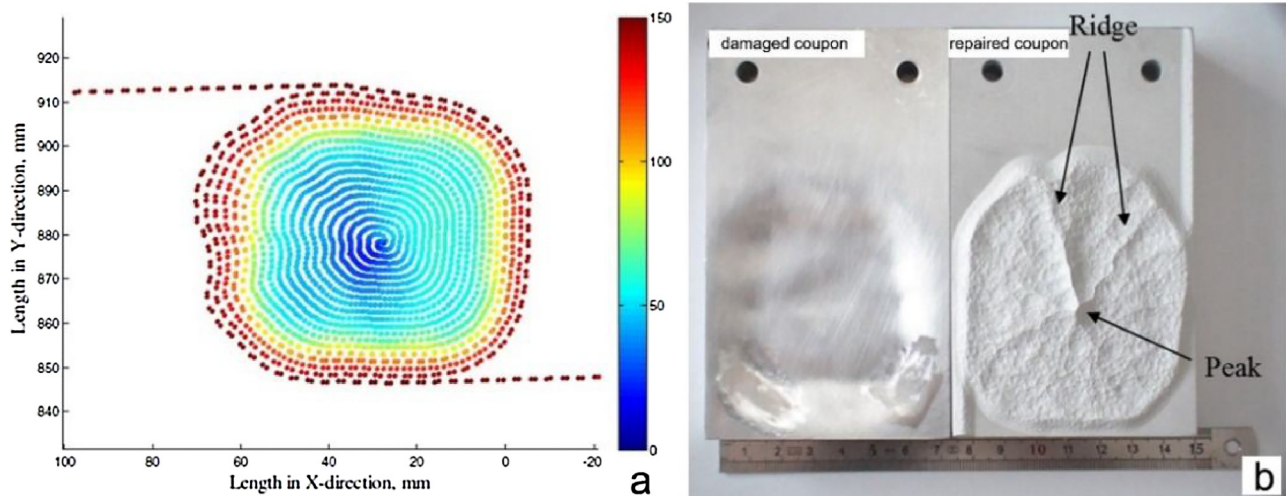


Fig. 15. (a) Nozzle traverse speed distribution along the spiral trajectory and (b) CSAM repaired coupon before final machining [74].

the chemical reaction at the inter-particle boundaries is more prominent at higher particle impact velocities, resulting in improved metallurgical bonding [8,83].

Heat treatment is also an effective tool to reduce deposit defects, and is particularly useful for mitigating defects at the inter-particle boundaries [81–92]. Fig. 16 shows a comparison of the microstructure of an etched copper deposit in the as-fabricated and annealed states, respectively [93]. The inter-particle boundaries can be clearly seen in the as-fabricated sample shown in Fig. 16a. After annealing, recrystallization takes place both within the particles and across the inter-particle boundaries, helping to repair the defects at inter-particle boundaries. As a result of the annealing process, the grain structure evolves to fine equiaxed grains. The inter-particle boundaries become less visible and in some cases are completely eliminated, as shown in Fig. 16b [81,94].

### 3.2. Properties of as-fabricated deposits

Table 3 summarizes the properties of CSAM copper deposits in their as-fabricated and heat-treated states. For comparison, the properties of bulk copper are also provided in the table. As-fabricated CSAM deposits normally have inferior mechanical properties when compared with bulk materials, due to a large number of defects within the deposits. They are very brittle and almost have no ductility. These effects are more prominent when the particle impact velocity is low [82–84]. Fig. 17a shows the stress-strain curve of a copper deposit produced using nitrogen as a propulsive gas, in the as-fabricated and annealed states. The poor mechanical properties (yield strength, ultimate tensile strength and elongation) of the deposit in the as-fabricated state are clear [83]. Besides the mechanical properties, other properties such as electrical conductivity [84,86–89,91,92] and thermal conductivity [90] are also typically lower when compared to those of bulk materials. This

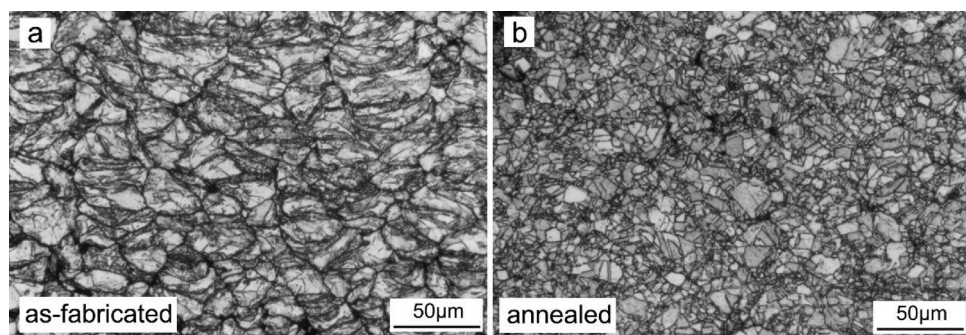


**Fig. 16.** Comparison of the microstructure of copper deposit (a) in the as-fabricated state and (b) in the annealed state. Annealing was performed at the temperature of 500 °C for 4 h [93].

**Table 3**

Summary of properties of CSAM copper deposits before and after heat treatment.

Gas	Parameters		HT condition				Hardness, Hv		UTS, MPa		EL, %		EM, GPa		EC, MS/m		TC, W/m·K		Ref.
					50		225–385		45–5		118		58		394				
	T, °C	P, MPa	T, °C	t, h	PG	AF	HT	AF	HT	AF	HT	AF	HT	AF	HT	AF	HT		
N <sub>2</sub>	800	3.0	300	4	Ar	–	–	294.6	338.4	0	0.68	84.3	104	–	–	–	–	[81]	
			400	4	Ar	–	–	268.7	33.1	103	–	–	–	–	–	–	–		
			500	4	Ar	–	–	245.8	41.0	100	–	–	–	–	–	–	–		
			700	4	Ar	–	–	178.4	24.5	111	–	–	–	–	–	–	–		
N <sub>2</sub>	500	3.0	200	5	air	150.0	149.3	161.6	176.0	5.8	–	–	–	–	–	–	–	[82]	
			300	5	air	–	–	120.6	179.5	6.2	–	–	–	–	–	–	–		
			400	5	air	–	–	94.1	200.0	7.4	–	–	–	–	–	–	–		
			500	5	air	–	–	68.6	240.4	45.4	–	–	–	–	–	–	–		
N <sub>2</sub>	305	3.0	200	1	vacuum	152.9	97.7	46	86	< 0.1	0.12	–	–	34.9	40.8	–	–	[83,84]	
			400	1	vacuum	–	–	77.9	171	0.51	–	–	–	49.0	–	–	–		
			600	1	vacuum	–	–	73.6	210	8.03	–	–	–	51.4	–	–	–		
He	300	2.5	200	1	vacuum	–	–	453	304	1.92	4.27	–	–	–	–	–	–	[83]	
			400	1	vacuum	–	–	–	278	20.99	–	–	–	–	–	–	–		
			600	1	vacuum	–	–	–	262	23.85	–	–	–	–	–	–	–		
He	500	2.4	150	1	air	108.0	90.3	320.0	295.8	2.4	4.0	–	–	–	–	–	–	[85]	
			200	1	air	–	–	85.1	256.8	15.8	–	–	–	–	–	–	–		
			300	1	air	–	–	56.4	244.2	50.1	–	–	–	–	–	–	–		
N <sub>2</sub>	300	3.0	200	1	–	150.1	98.1	–	–	–	–	–	–	35.7	41.5	–	–	[86]	
			400	1	–	–	79.1	–	–	–	–	–	–	–	50.0	–	–		
			600	1	–	–	74.8	–	–	–	–	–	–	–	52.8	–	–		
N <sub>2</sub>	450	2.2	300	1	air	122.6	–	–	–	–	–	–	–	–	17.6	29.7	–	–	[87]
			450	1	air	–	–	–	–	–	–	–	–	–	32.3	–	–		
			300	4	air	–	–	–	–	–	–	–	–	–	44.9	–	–		
			450	4	air	–	–	–	–	–	–	–	–	–	45.1	–	–		
			300	1	vacuum	–	86.7	–	–	–	–	–	–	–	49.3	–	–		
Air	400	2.0	450	1	vacuum	–	–	–	–	–	–	–	–	–	49.6	–	–		
			400	1	vacuum	169.3	109.1	–	–	–	82.7	94.0	–	30.2	–	–	–	[88,89]	
			600	1	vacuum	–	93.81	–	–	–	–	99.4	–	33.4	–	–	–		
			800	1	vacuum	–	72.4	–	–	–	–	115.0	–	36.5	–	–	–		
Air	400	0.6	200	1	vacuum	99.5	75.3	–	–	–	–	–	–	–	–	125.2	164.5		
			400	1	vacuum	–	74.0	–	–	–	–	–	–	–	–	262.6	[90]		
			600	1	vacuum	–	55.3	–	–	–	–	–	–	–	–	320.6			
N <sub>2</sub>	400	3.0	400	2	Ar	145	80	–	–	–	–	–	–	38.6	52.7	–	–	[91]	
Air	540	0.6	400	2	Ar	106	62	–	–	–	–	–	–	26.7	40.0	–	–		
Air	600	0.9	400	2	H <sub>2</sub>	235.7	76.5	–	–	–	–	–	–	29.3	48.6	–	–	[92]	

T: temperature; P: pressure; t: time, PG: protective gas, AF: as-fabricated, HT: heat treatment, UTS: ultimate tensile stress, EL: elongation, EM: elastic modulus, EC: electrical conductivity, TC: thermal conductivity.

is due to defects such as particle boundaries acting as barriers which prevent the transportation of current and heat through the deposits. Conversely, the hardness of the as-fabricated deposits is generally higher than that of bulk materials due to the work hardening effect which occurs during the deposition process [82,84–92].

However, when sprayed using high particle impact velocities, the as-fabricated deposits show improved mechanical properties when compared to those sprayed using low particle impact velocities [81,83,85]. The strength of high particle velocity cold spray deposits has been shown to be equal or even higher than annealed deposits and

bulk materials, as listed in Table 3 [81,83,85]. Fig. 17b shows the stress-strain curve of a copper deposit in its as-fabricated state and annealed state produced with helium [83]. It is clearly seen that the as-fabricated copper deposit had higher tensile strength than annealed deposits. The reason for this phenomenon can be attributed to two factors. Firstly, increasing the impact velocity results in the improvement of inter-particle bond strength. Secondly, increasing levels of grain refinement caused by the higher levels of plastic deformation will increase the strength of the deposited particles, and thus the whole deposit [95,96].

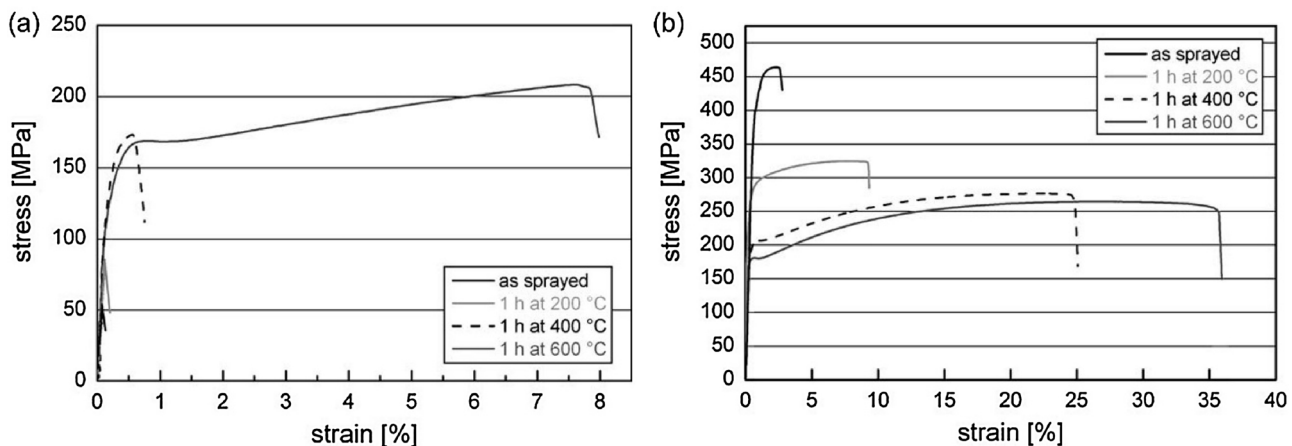


**Fig. 17.** Stress-strain curve of copper deposit before and after annealing: (a) produced by nitrogen, and (b) produced by helium [83].

### 3.3. Properties of heat-treated deposits

Heat treatment is the most effective way to enhance the properties of CSAM deposits. By annealing the as-fabricated deposits, both tensile strength and ductility are significantly improved, due to the mitigation of the defects in the deposits, as shown in Fig. 17a [82–84]. Higher annealing temperature and longer annealing time tend to cause to more significant improvement in properties. The tensile strength and elongation of annealed copper deposits can reach the same level as the bulk copper under proper annealing conditions. Similarly, the elastic modulus also improves after annealing due to the decrease in deposit defects [81,88,89]. However, because of the occurrence of recrystallization during the annealing process, work-hardened deposits are softened. As a result, the hardness of annealed deposits is normally lower than that of as-fabricated ones [82,84–92]. Furthermore, as the inter-particle boundaries are repaired, the barriers for the transportation of heat and current are eliminated. Hence, annealed CSAM deposits have better electrical conductivity [84,86–89,91,92] and thermal conductivity [90]. For copper, annealed deposits can achieve more than 90% of the electrical and thermal conductivity levels of bulk material.

However, under high particle impact velocity, heat treatment will improve the ductility but reduce the tensile strength of CSAM deposits, which is quite similar to the heat treatment of bulk materials [81,83,85]. This is because the as-fabricated deposits under high particle impact velocity already gain sufficiently high strength due to the absence of defects and strengthening effect by grain refinement. Heat treatment, therefore, has no use for healing the defects but only contributes to the recrystallization of the deposits.

## 4. Machining of CSAM deposits

### 4.1. Machinability of CSAM deposits

CSAM typically leaves a rough, undulating and porous surface after fabrication. In many applications, such as in the repair of a worn surface, the as-fabricated surface is not suitable for immediate use, either due to surface finish or dimensional accuracy requirements. This necessitates the use of a machining or finishing process. To date, relatively little research has been undertaken into the machinability of CSAM materials [42,43,97–99]. In general, CSAM products are suitable for normal machining processes. As examples, Fig. 18 shows three CSAM products made using a high pressure cold spray system located in Trinity College Dublin (TCD), which were machined into finished parts using normal machining processes. The aluminium alloy tube shown in Fig. 18a was finished by turning; the aluminium alloy flange shown in Fig. 18b was finished by turning and drilling; the copper cuboid shown in Fig. 18c was finished by milling. These cases clearly demonstrate the

suitability of normal machining processes for CSAM products.

When understanding the machining of CSAM deposits, it is important to recognize that unless the deposit has been brought to full density or high ductility, through proper annealing, hot isostatic pressing (HIP) or a similar method, it will machine similarly to a porous or cast material. As CSAM deposits are an amalgamation of individual particles, there will be variations in density and levels of work hardening within the deposit, with the potential for small oxide inclusions [100]. This will cause variations in the mechanical and thermal loads experienced by the cutting tool. Many comparisons can be made between the machining of CSAM deposits and materials produced through powder metallurgy [101] and fusion-based additive manufacturing [102–104], which are acknowledged as more problematic to machine when compared to bulk materials. Fig. 19 shows a comparison of the chip formation mechanisms between bulk aluminium and CSAM aluminium with and without annealing during machining [98]. Fully dense bulk aluminium generally results in continuous chip formation during machining as shown in Fig. 19a. Annealed CSAM aluminium which has good ductility forms discontinuous chips, but otherwise machines similar to the bulk material (Fig. 19b). However, for the as-fabricated CSAM aluminium as shown in Fig. 19c, due to the poor inter-particle bonding and little particle deformation, the cutting process resembles that of a sintered material, with inter-particle bonds being broken and no chips being formed. The surface finish after machining of any such material would be porous and undulating, though some smearing and densification of the surface may be observed [105]. Thus, the machinability of a CSAM product is dependent upon the density and ductility of the deposit created.

Other issues which are of interest in the machinability of CSAM product are the potential for debonding of the deposits if overly aggressive cutting parameters are used, or if a significant portion of the bond area is removed during machining. If it is necessary to remove the deposits from the substrate to achieve the geometry required, this should be carried out first, as the CSAM product may distort due to residual stresses after debonding.

### 4.2. Cutting forces during the machining of CSAM deposits

Cutting forces during the machining of porous CSAM deposits will typically be lower than that of bulk material, but with more variation during cutting [98]. Porous materials manufactured using other techniques typically show lower but more variable cutting forces [106]. The lower magnitude of the forces is at least partially attributable to the lower stiffness of porous materials [107], while the variation is due to the partially discontinuous cutting action experienced as the tool disengages and then re-engages when passing through pores. CSAM deposits with higher ductility will show less variation in cutting forces,

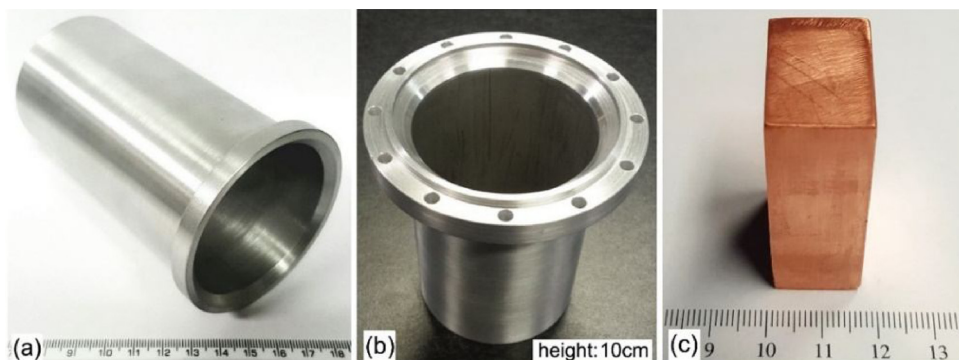


**Fig. 18.** CSAM tube machined into a finished part fabricated in TCD. (a) aluminium alloy tube, (b) aluminium alloy flange, and (c) copper cuboid.

while deposits with lower porosity will show higher cutting forces.

#### 4.3. Tool wear during the machining of CSAM deposits

Little to no research has been carried out into tool wear during the machining of CSAM deposits. It can be expected that, due to the discontinuous nature of the machining process, tool wear will be greater than that observed when machining bulk material. The use of tamping materials in the CSAM process such as alumina, which are typically very hard, will cause excessive tool wear during machining [108]. This has been observed by the authors in the preparation by milling of tensile test samples from CSAM diamond-reinforced metal matrix composite. 5–10 tools were required per sample, with tool life being measured in seconds. Further research work is required to characterize the tool wear mechanisms in CSAM materials.

#### 4.4. Properties and microstructure of CSAM deposits after machining

Turning is the primary machining operation for the finishing of cylindrical CSAM deposits. For as-fabricated CSAM deposits, turning may not be suitable for removal of all excess material. Some deposits will fail at inter-particle boundaries and separate from the deposit or substrate as a small clump of particles, due to weak inter-particle bonding. As a consequence, the surface of as-fabricated CSAM deposits after turning may have a smeared surface with high surface roughness, as shown in Fig. 20a [98]. By increasing particle impact velocity or using a heat treatment process prior to machining, the surface roughness of the turned CSAM deposits can be significantly reduced due to the improved inter-particle bonding, as shown in Fig. 20b–d [98]. In addition, turning also removes the compressive residual stress of the as-fabricated CSAM deposits and introduces tensile stress to machined surface of the deposits [99].

Milling is required for the finishing of CSAM deposits without axial symmetry. In recent work by the authors, milling was found to influence the deposit microstructure close to the machined surface. Fig. 21

shows the cross-sectional image of a CSAM aluminium deposit after milling. Clearly, the milling process compresses the top layer of the deposit, making it much denser than the original deposit. In addition, milling tends to break the brittle CSAM deposit due to the large cutting force. Improper milling parameters will cause cracks, fracture and delamination of the CSAM deposit [99,109]. Therefore, careful selection of machining parameters is required to achieve a satisfactory finish. Careful inspection for cracks and damage should be carried out on the CSAM product after machining.

Currently, investigations on the properties and microstructure of CSAM deposits after machining are still very limited. Therefore, more studies on this topic are needed in the future to fully clarify the effect of machining methods and machining parameters on the grain structure, microstructure and properties of CSAM deposits.

### 5. CSAM for fabricating free-standing components

#### 5.1. Rotational structures

A broad range of components have rotational structures (e.g. tubes, flanges and cylinder walls). CSAM has the capability to fabricate such components. Using an external spindle to hold the mandrel substrate, the rotational structure can be easily fabricated through a simple spray strategy. For instance, as shown in Fig. 18b, the aluminium flange was successfully fabricated for an Irish company (Moog) in the authors' lab in TCD. Aluminium was first deposited onto an aluminium tube which was held and rotated by a spindle, then the as-fabricated raw product was post-machined using turning and drilling (including a cut which crosses the interface between the substrate and CSAM deposit) to finalise the flange feature. Tests of the mechanical properties have demonstrated that this method of manufacture completely meets the requirements of the company. A similar CSAM copper flange is also shown in Fig. 22 [110]. Here, it should be noted that CSAM is only able to produce a rough structure rather than net-shape structure. Thus the as-fabricated CSAM deposits normally require a post-machining

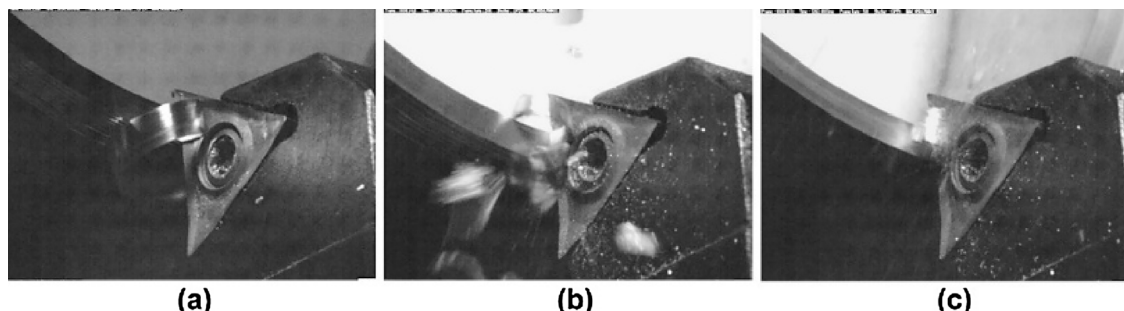


**Fig. 19.** Comparison of the chip formation mechanisms between bulk and CSAM aluminium with and without annealing during post-machining. (a) bulk material, (b) annealed CSAM deposit and (c) non-annealed CSAM deposit [98].

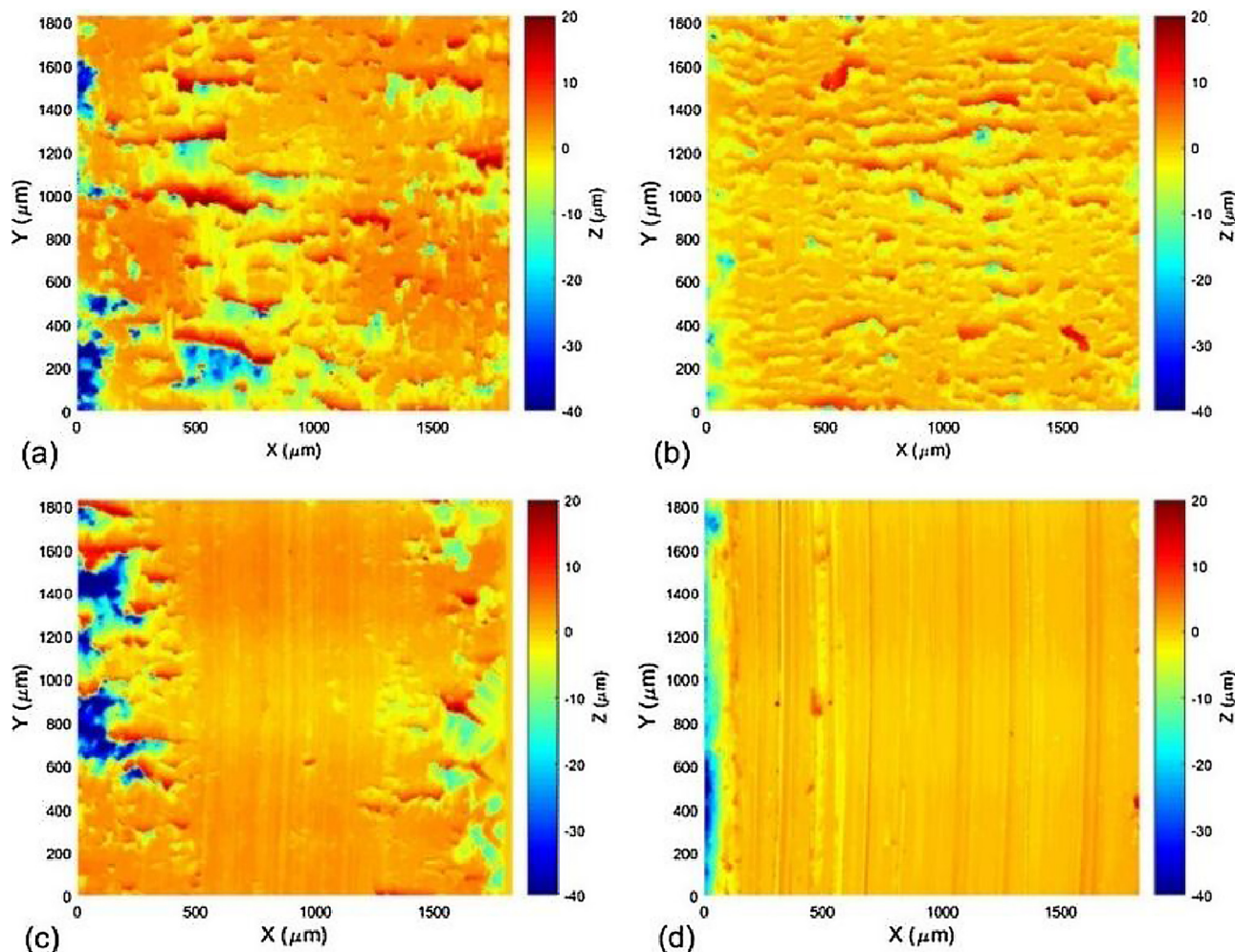


**Fig. 20.** White light interferometer maps of turned surfaces of aluminium deposits. (a) as-fabricated deposit produced by nitrogen, (b) heat-treated deposit produced by nitrogen, (c) as-fabricated deposit produced by helium, and (d) heat-treated deposit produced by helium [98].

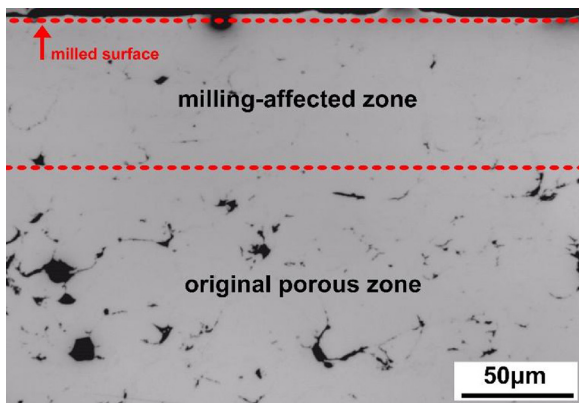


**Fig. 21.** Cross-sectional image of a CSAM pure aluminium deposit after milling. The aluminium deposit was fabricated using nitrogen with the pressure of 3 MPa and temperature of 400 °C by the cold spray system in TCD.

(subtractive manufacturing) process to produce the required shape. This is not only applicable to rotational structures, but also to all CSAM products.

Metal cylinder outer and inner walls can also be produced using CSAM [43,111–116]. The fabrication process is similar to the flange fabrication, particularly for the case of an outer wall. Fig. 23a provides an example showing a 1/10 scaled canister for disposal of CANDU spent

fuels, fabricated using CSAM [112]. A 10 mm copper layer with a porosity of 0.3%, density of 8900 kg/m<sup>3</sup> and oxygen content of 0.019% (compared to 0.02% oxygen content of the feedstock copper powder) was deposited onto the cast iron cylinder, with good tensile strength, mechanical stability and thermal properties. For certain components, the mandrel substrate is not needed and has to be removed during the post-machining process. An instance of this kind of product is provided in Fig. 23b, showing a CSAM tantalum-10 tungsten alloy donor tube used for the fabrication of gun barrel liners [111]. The tantalum-10 tungsten alloy layer was deposited onto a cylindrical aluminium mandrel substrate, after which the inner mandrel was removed using deep drilling, honing, and a brief soak in dilute sodium hydroxide.

For the fabrication of inner walls, the manufacturing procedure varies according to the inner diameter. If the inner diameter is sufficiently large that the conventional cold spray nozzle and its holding accessories can be placed within the component, the fabrication process is same as producing the outer wall. But in circumstances where the component is not large enough to accommodate a cold spray nozzle, the nozzle has to be slightly inclined to fit the limited space, at the expense of lower deposit quality due to the spray angle. An example is provided in Fig. 24a, showing a copper inner wall of a pressure ring from a food processing machine, which was fabricated using CSAM [116]. In this case, the nozzle had to be inclined to the target substrate during the fabrication due to the limitation of the inside diameter of the component. Furthermore, if the inner diameter is too small to accommodate a normal cold spray nozzle, a specially-designed short cold spray nozzle



Fig. 22. Digital photos of a CSAM copper flange [110].

can be used [115,117]. Fig. 24b shows a short cold spray nozzle designed for small-diameter inner walls. The nozzle has a length of only 6.5 mm, far less than a normal cold spray nozzle. Fig. 24c shows a copper inner wall on a metal tube with the diameter of 80 mm fabricated using this short nozzle [115].

CSAM is also capable of producing other special rotational structures such as cones and gears, as shown in Fig. 25 [115,118]. To fabricate such structures, an elaborate design and scanning trajectory must be developed before manufacture. Nozzle traverse speed, scanning step and trajectory should be linked to the spindle axis. There are very few studies on such special rotational structures, and therefore this topic may be a future research focus.

### 5.2. Complex structures

A combination of CSAM and conventional subtractive manufacturing has recently shown great potential in fabricating components with complex structures. Fig. 26 shows a component with a complex structure which was manufactured using CSAM [71]. To fabricate this component, the additive material was first deposited onto a specially designed substrate. After spraying the substrate was removed and only the CSAM part remained. Through a combination of CSAM and subtractive manufacturing, a complex component was produced. The

challenge of this process is the design of the substrate to ensure ease of removal, and to minimize post-process machining. Based on this technique CSAM can also be used to modify an existing component. Fig. 27 shows the modification process of adding a new part onto a bearing cap via CSAM. As can be seen, a completely new component was obtained after CSAM. Visually, there is no obvious boundary between the new part and original component. The new component passed the customer's quality and performance specifications [119], proving the feasibility of CSAM for this application. Fabrication of such complex structures is very important to CSAM technology as this can significantly broaden the application areas. Therefore, further investigation is suggested in this area of CSAM.

CSAM can also produce array structures. As shown in Fig. 28a, the fabrication process needs a specially designed mask to prevent the deposition of redundant materials to allow only the deposition of the desired pattern. An example of a CSAM array structure is the pyramidal fin arrays used for a compact heat exchanger, as shown in Fig. 28b [120–127]. By adjusting the standoff distance and design scheme of the wire mask, the fin array shape and density can be accurately controlled [120,125–127]. The thermal and mechanical tests suggest that the CSAM fin arrays had superior thermal performance than traditional straight (rectangular) fins, due to the higher convective heat transfer coefficients [46,125,126]. Further studies have suggested that heat transfer performance can be improved by increasing the fin height, increasing fin density, or by using staggered configurations at the expense of a higher pressure loss [120,123]. In addition, mask-assisted CSAM also can be used to fabricate chip heat sinks, metal markings, or other products with special patterns [18,128,129].

### 6. CSAM for repairing damaged components

Component damage frequently occurs after long service times due to corrosion, wear, fatigue, or other causes. Damaged components often cannot be reclaimed or repaired, and have to be replaced due to the lack of effective restoration methods. CSAM is a cost-effective process that has shown great potential in the repair of damaged components, due to its capability to avoid any thermal damage to the underlying substrate material, and unique ability to retain the original properties of the feedstock powder. During the past decade, CSAM has been successfully applied to repair a variety of corroded and damaged components in various fields. Similar to other restoration techniques, the feedstock for CSAM cannot be deposited on the damaged component directly because of the complex surface topography, and the potential for the contaminated surface of the damaged area to compromise bond strength. Pre-machining on the damaged zone is necessary to reconstruct the damaged surface. Surface treatment is then conducted on the reconstructed surface with milling, grinding, or grit-blasting to prepare a clean and smooth surface which is suitable for CSAM [130–132]. After deposition, the as-coated components also have to be post-machined to their original dimensions. The standard restoration process normally includes the following four stages: pre-machining of the damaged zone,

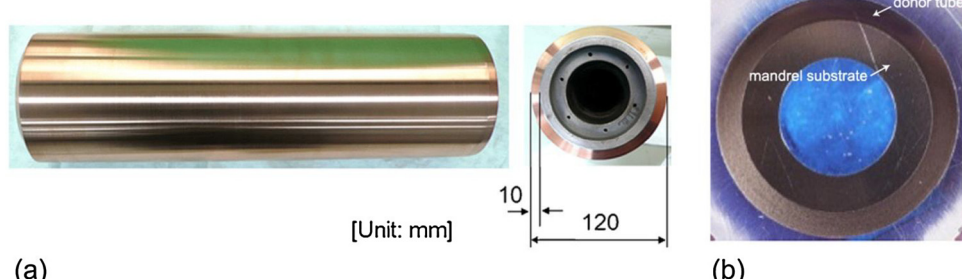
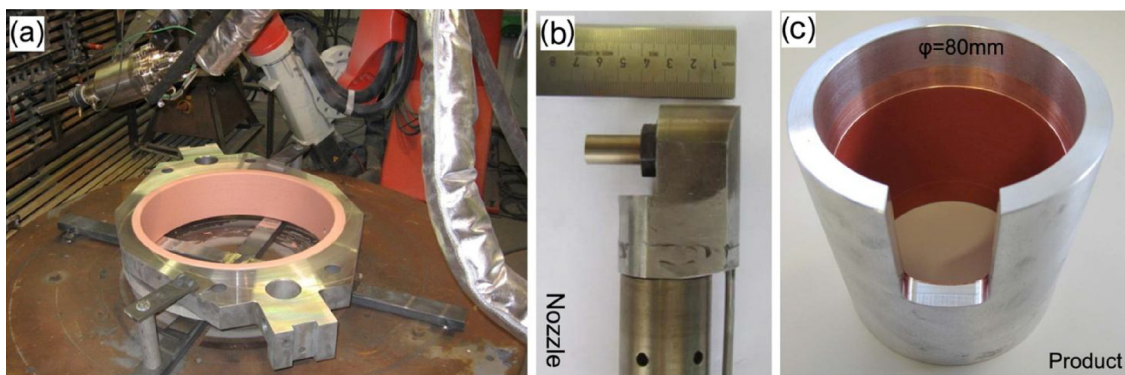
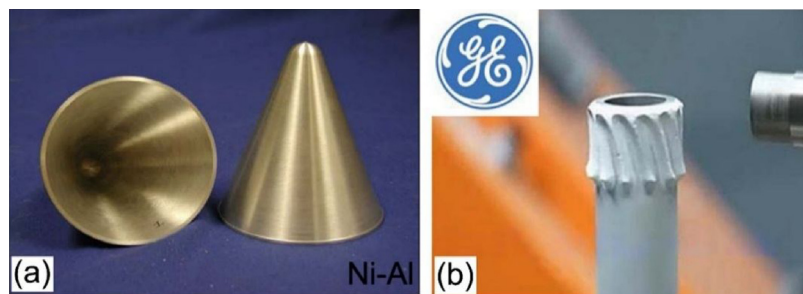


Fig. 23. Digital photos of CSAM rotational structure: (a) scaled canister for disposal of CANDU spent fuels and (b) tantalum-10 tungsten alloy donor tube used for the gun barrel liners [111,112].



**Fig. 24.** Digital photos of CSAM rotational structure: (a) an inner wall of a pressure ring for food processing machine, (b) a small-size cold spray nozzle and (c) an inner wall of small-space cylinder tube [115,116].



**Fig. 25.** Digital photos of CSAM components with complex structures: (a) cone structure, and (b) gear [115,118].

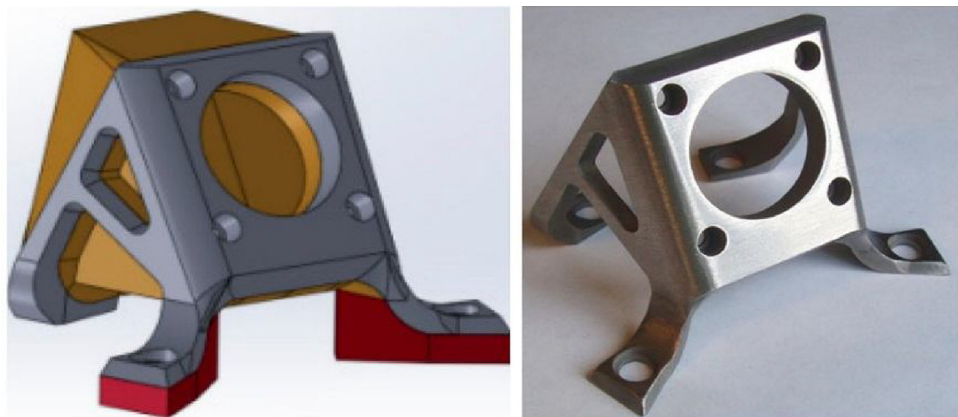


**Fig. 26.** Component with complex structure made by CSAM [71].



**Fig. 27.** Modification process of adding a new part to a bearing cap via CSAM [119].

material deposition, post-machining on the back-filling material, and performance testing. These steps are illustrated in Fig. 29.

#### 6.1. Corrosive and erosive damage restoration

Among all applications of CSAM, the repair of aircraft components is potentially the most promising due to the severe corrosion and wear that aerospace components are subject to. This is due to the exposure of

these components to high-speed impact, high-speed rotation and humid air. Magnesium and magnesium alloys possess many merits (e.g. high stiffness, low density, high thermal conductivity and excellent machinability) over other metals, and thus have been widely used for the fabrication of aircraft transmission gearboxes. However, as an electro-chemically active material, magnesium components tend to corrode due to the anodic reaction with other metallic materials. Therefore, magnesium gearboxes frequently suffer from electrochemical corrosion in

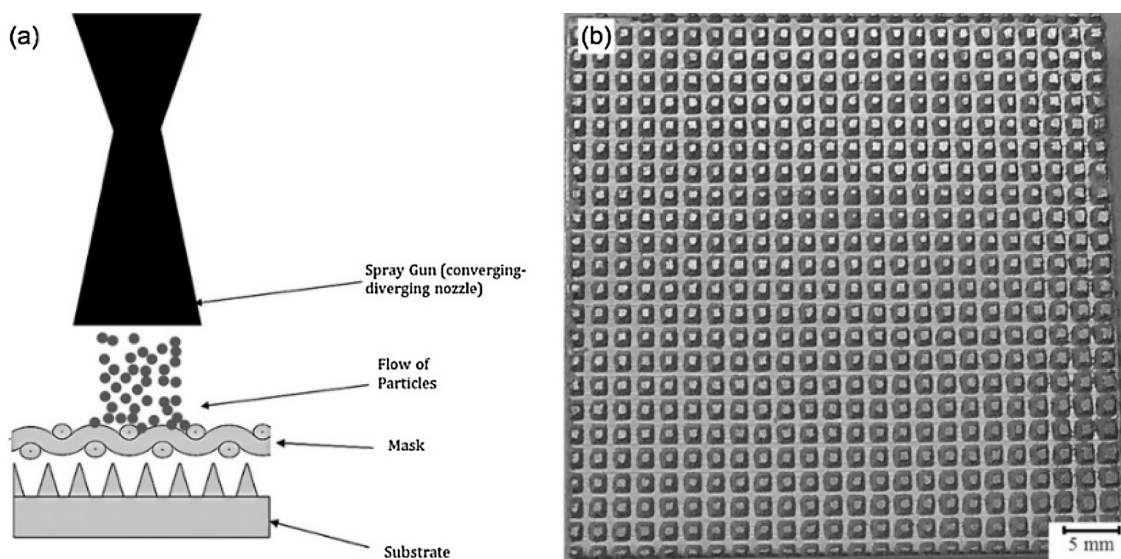


**Fig. 28.** CSAM pyramidal fin arrays heat sink. (a) schematic of the fabrication process and (b) digital photo of a CSAM fin array heat sink.



**Fig. 29.** Restoration procedure via CSAM.

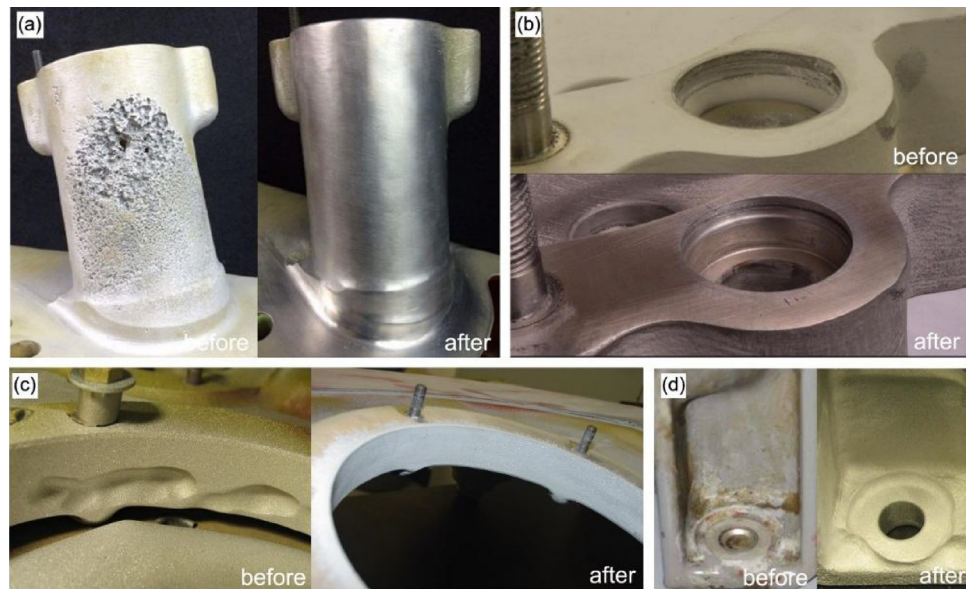


**Fig. 30.** Comparison between damaged and repaired components via CSAM: (a) S-92 helicopter gearbox sump, (b) oil tube bores in CH47 helicopter accessory cover, (c) UH-60 helicopter gearbox sump and (d) UH-60 rotor transmission housing [133–135].

service. Such corrosion significantly reduces the component lifetime, increasing the maintenance cost and potential failure risk. It is of great importance to properly repair the corroded zone and bring the restored component back to a serviceable condition. By using CSAM, the corroded part of the transmission gearbox can be repaired with aluminium or aluminium alloy materials. Fig. 30 shows CSAM being used for repair

of damaged transmission gearboxes [133–135]. Mechanical and corrosion tests on the repaired components confirm that the back-filled aluminium and aluminium alloy materials had excellent adhesive strength, wear-resistance, and corrosion-resistance. These restored components are suitable to be returned to flying [136–138].

Aluminium and aluminium alloys are also widely used in aircraft,

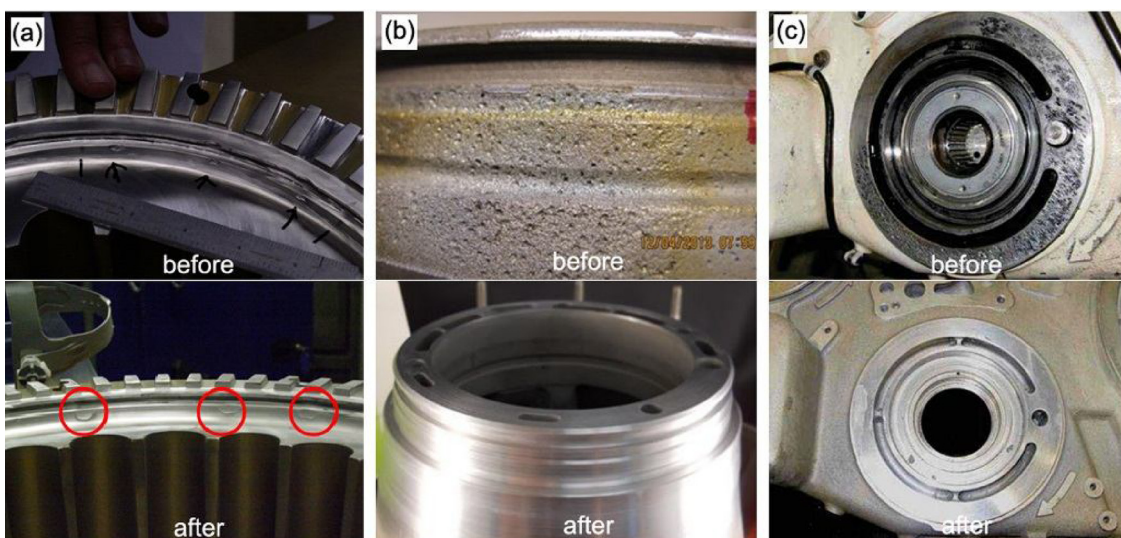


**Fig. 31.** Comparison between damaged and repaired components via CSAM: (a) AH-64 helicopter mast support, (b) F18-AMAD gearbox and (c) front frame of T-700 engine [135,139,140].



**Fig. 32.** Comparison between damaged and repaired components via CSAM: (a) internal bore surface of a navy valve actuator and (b) oil pump housing of Caterpillar engine [141,142].



**Fig. 33.** Restored B737 nose wheel steering actuator barrel via CSAM [133].

marine and automotive components due to their low density, high tensile strength, good formability and excellent corrosion resistance. In the aerospace industry, the helicopter mast support is an example of a major component which is commonly manufactured using aluminium alloys. Corrosion pitting on the snap ring groove surface is a typical form of damage that helicopter mast supports can suffer from during

their service life. When the pitting damage exceeds a criterion, the mast support must be repaired or replaced. Rather than scrapping the mast support, CSAM can be used to repair the damage and return the component to service. Fig. 31a shows a comparison between a damaged and repaired snap ring groove surface of a mast support [139]. The detailed restoration procedure involves the blending out of corrosion pits, then backfilling the removed part by CSAM deposition of aluminium alloy, and finally post-machining the as-repaired component. Similar CSAM restoration work of aircraft aluminium alloy components is shown in Fig. 31b and c [135,140]. In the marine industry, CSAM has been successfully applied to the repair of corroded internal bore surface of navy aluminium alloy valve actuator without thermally affecting the base material, showing improved capabilities when compared to other traditional repair methods (i.e., tungsten inert gas welding, metal inert gas welding, and laser cladding). Fig. 32a shows a comparison between the damaged and repaired actuator. The actuator repaired using CSAM has passed all property tests and is now back in service [141]. Moreover, in the automotive industry, CSAM has been applied to repair corroded oil pump housings of Caterpillar-3116 and Caterpillar-3126 engines with aluminium alloy (Fig. 32b). It was reported that more than 30 corroded pump housings were restored via CSAM from 2012 to 2013 in Moscow. All of these reconditioned components have returned to service without any failure reports so far [142].

The nickel superalloy Inconel is another important material that is frequently used in aerospace industry, due to its excellent mechanical properties at high temperatures and resistance to corrosion. Aircraft components made using nickel alloys suffer from significant mechanical and thermal loading during flight. This results in severe wear and corrosion of these components, and thus reductions in their service lifetimes. Nose wheel steering actuator barrels manufactured using nickel alloy and are located in the front of the aircraft, which exposes these components to moisture and other harsh environments when the landing gear is extended. These negative factors affect the component joints, resulting in corrosion of landing gear. By using CSAM, a corroded B737 nose wheel steering actuator barrel was repaired with CSAM deposition of nickel alloy. Fig. 33 shows the comparison between a damaged and repaired B737 nose wheel steering actuator barrel. The corroded surface becomes smooth after repair, without any pits and cracks [133].

## 6.2. Mechanical damage restoration

Mechanical defects caused by fatigue, accidental impact, overhaul

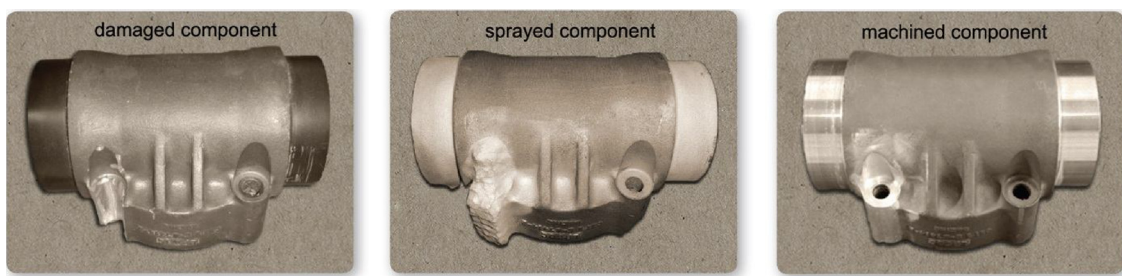


Fig. 34. Restoration process of a mechanically damaged flap transmission tee box housing of an aircraft via CSAM [133].

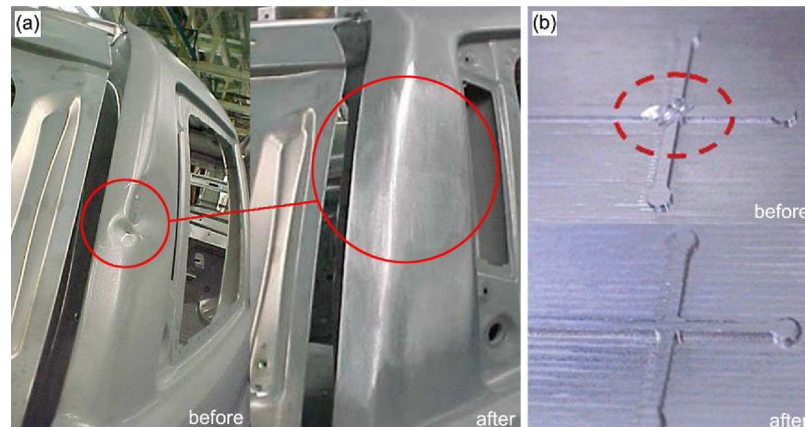


Fig. 35. Comparison between damaged and repaired components via CSAM: (a) a large cast automotive part and (b) a mold [97,143].

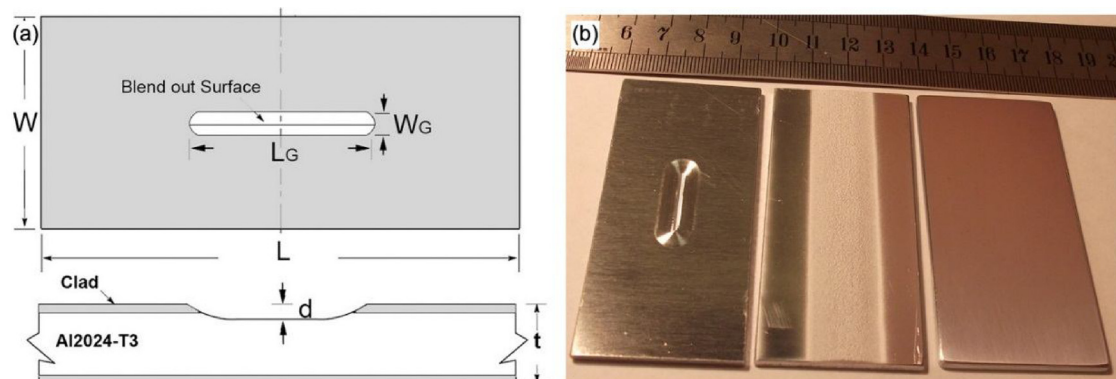


Fig. 36. Repair result of aluminium cladding layer on the aluminium alloy panel with self-machined damage via CSAM: (a) schematic of the self-machined damage and (b) restoration process [148].

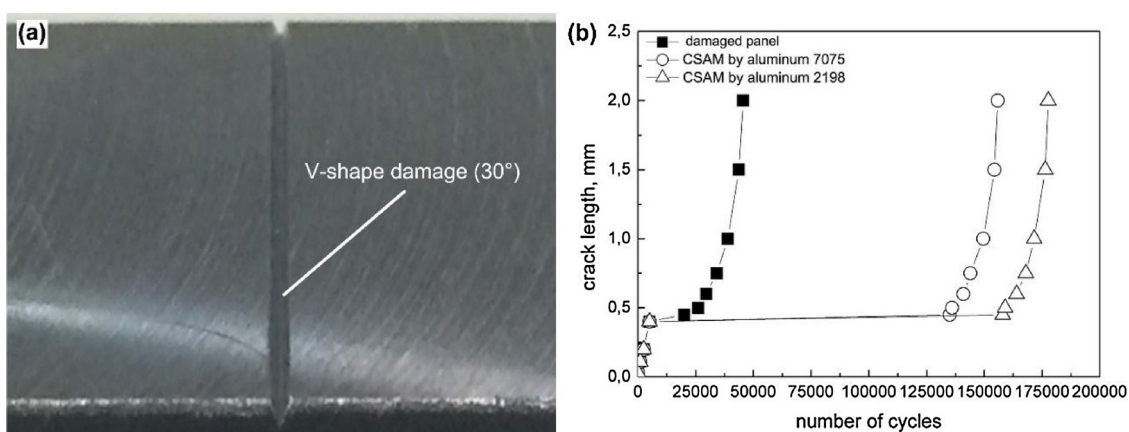
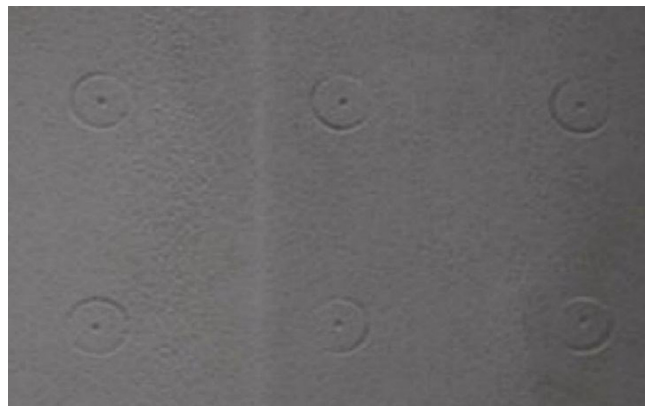


Fig. 37. (a) Digital photo of the machined notch made on the aluminium alloy 2099 panel surface, (b) crack length versus the number of loading cycles [149].



**Fig. 38.** Cold spray deposit over the simulated fuselage fasteners.

or improper operation are another type of damage that components may experience. This type of mechanical damage can also be repaired by CSAM. Fig. 34 shows the restoration process of a mechanically damaged flap transmission tee box housing of an aircraft via CSAM [133]. The damaged component was repaired to the original condition it was in prior to the damage occurring. CSAM is also used to repair severe mechanical damage on large cast automotive parts, as can be seen in Fig. 35a [143]. Restoration of damaged molds is also in the scope of CSAM, as shown in Fig. 35b. The repaired mold presented similar results during the cutting force test to bulk material, and even better wear-resistance performance than the original component [97].

### 6.3. Damaged metal sheet restoration

Commercial and military aircraft skins are primarily manufactured from aluminium alloy sheet, with additional aluminium cladding layer to prevent corrosion. During routine flight, the aircraft skin has a high probability of suffering erosion and scratch damages due to high-velocity impact of dust and debris. The damaged area acts as a weak point, preferentially allowing the corrosion to penetrate through the protective aluminium clad layer, down to the base aluminium alloy. Once the base aluminium alloy is seriously corroded, the maintenance and failure cost will be very high. Therefore, it is necessary to repair the damaged aluminium cladding before the corrosion penetrates to the underlying base material. Some thermal spray technologies have been used to repair the damaged aircraft skin; however, the thermal sprayed coatings suffer from high porosity, high oxidation, and phase transformations during deposition. Most importantly, upon impact the high-temperature feedstock may have adversely effected the underlying base material, significantly degrading the aircraft skin performance [144]. CSAM has the potential to carry out this repair without damaging the underlying base material [145–147]. Fig. 36 shows the repair of an aluminium cladding layer on an aluminium alloy panel via CSAM [148]. Visually, the damaged area is completely filled by the aluminium deposit without any obvious distinction from the surrounding aluminium cladding. Mechanical tests of the repaired sample suggest that the deposit

hardness was higher than the original aluminium cladding, and the fatigue resistance of the repaired sample was improved. In addition, corrosion test reveals that the CSAM aluminium deposited on the damaged aluminium cladding provided an effective protection to the aluminium alloy base material, despite slight corrosion propagating from the repair edge in some cases [148].

In a recent study, fatigue tests of CSAM repaired aluminium alloy 2099 panels were conducted [149]. Fig. 37a shows the digital photo of the machined notch on the aluminium alloy 2099 panel surface. The notch was repaired by CSAM with aluminium alloys 2198 and 7075, respectively. Crack growth tests were then performed on these repaired panels [149]. Fig. 37b shows the crack length as a function of the number of loading cycles for the damaged and repaired aluminium alloy panels. The crack length of the repaired panels was decreased by a factor of 6–7 when compared to the damaged panel. This is due to the strong adhesion between the CSAM deposit and the underlying substrate preventing crack initiation and growth. These results clearly demonstrate the feasibility of CSAM restoration in improving the fatigue performance of damaged sheets.

Aircraft fuselages also suffer from Multi Site Damage (MSD) issues. For nearly all kinds of aircraft, the fuselage is fabricated through lap joints of aluminium alloy skin panels. Therefore, failures and accidents associated with lap joints may occur after extended service lives. Fastener bore corrosion will take place through the interface between fastener and skin, despite the edge sealing between mating panels. In addition, multiple fastened strip repairs also act as a weak point, preferentially inducing the generation of cracks. These potential risks cumulatively cause the MSD on the aircraft skin. By using CSAM combined with standard sealant, the invasion of the moisture into the joint from the interface between mating panels and also between fasteners and aircraft skin can be prevented [145,146,150]. Fig. 38 shows a digital photo of CSAM deposit over the simulated fuselage fasteners. It is shown that the surface of the fasteners are completely sealed by the CSAM deposit. Subsequent fatigue testing results indicate that the deposit remained intact even when the underlying fuselage joint skin experienced MSD. Furthermore, CSAM has shown great potential in the repair of cracks caused by MSD, which helps to enhance the fuselage structural integrity [145–147].

Aircraft propeller blades also suffer from serious erosion due to high-velocity impact by dust, debris and water droplets in service. Moreover, relatively large debris impacts during aircraft taking off and landing will lead to more severe damage to the blade surface. The current method used to repair this damage is simply to grind the eroded blade to a level that the damage is removed. By using CSAM, the material removed during the grinding process can be filled, which allows for the original blade dimensions to be restored. Fig. 39 illustrates the repair process of aluminium alloy blades via CSAM. The restored blades have passed an extensive airworthiness test program and are currently back in service [151].

## 7. Current challenge and future perspectives

Cold spray technology has shown great potential in additive



**Fig. 39.** Restoration process of aluminium alloy blades via CSAM [151].

manufacturing, both for the fabrication of individual components and the repair of damaged components. This is due to its ability to retain the original feedstock properties and prevent adverse influence on the underlying substrate materials. A variety of components have been successfully fabricated or repaired via CSAM during the past years. Properties and performance tests have confirmed that the mechanical properties of CSAM products are sufficient to be used in a wide variety of applications. Despite the merits highlighted so far, CSAM is still facing many challenges:

- 1 The currently applied materials for CSAM are mainly copper and aluminium, which are very easy to deposit and machine. In future work, more materials need to be implemented and tested, such as titanium, stainless steel, and metal matrix composites. These materials are either hard or have a high strength-to-weight ratio, and thus are difficult to produce with acceptable mechanical properties. More trials and investigations on these materials will aid in evaluating if these materials are suitable for CSAM.
- 2 A thorough understanding of the spraying parameters is another research focus in the future, as currently their effects on the deposit properties are not entirely agreed upon. Particularly, the effect of scanning steps and standoff distance on the deposit mechanical properties needs further investigation. A standard manufacturing strategy for achieving optimal deposit properties should be developed.
- 3 The isotropic and anisotropic properties of CSAM deposits are not fully understood, and require a thorough investigation. In addition, development of more advanced post-treatment methods (e.g., laser surface treatment, hot isostatic pressing, surface shot-peening) for improving the properties of CSAM products would aid in improving the capabilities of CSAM.
- 4 Investigations on the post-machining process of CSAM products are very rare at the time of writing. As CSAM products normally require post-machining, this should be another area of focus for future research.
- 5 Currently, only a small number of publications have studied complex structure fabrication. The application of CSAM for the fabrication of complex components is an interesting and challenging subject. Particular attention should be paid to the substrate and mask design for the purpose of minimizing post-machining processes.
- 6 The current applications of CSAM are mainly concentrated in the aerospace sector. It is suggested that other application fields should be explored in future work.

## Acknowledgments

The authors would like to thank the financial support from Irish Research Council (GOIPD-2017-912) and Enterprise Ireland (CF20144626).

## References

- [1] A.P. Alkhimov, V.F. Kosarev, N.I. Nesterovich, A.N. Papyrin, 1980. Method of applying coatings (SU 1618778).
- [2] A.P. Alkhimov, V.F. Kosarev, A.N. Papyrin, A method of cold gas-dynamic spray deposition, Dokl. Akad. Nauk SSSR. 315 (1990) 1062–1065.
- [3] H. Assadi, H. Kreye, F. Gärtner, T. Klassen, Cold spraying — A materials perspective, Acta Mater. 116 (2016) 382–407, <http://dx.doi.org/10.1016/j.actamat.2016.06.034>.
- [4] R.N. Raolison, Y. Xie, T. Sapanathan, M.P. Planche, R. Kromer, S. Costil, et al., Cold gas dynamic spray technology: a comprehensive review of processing conditions for various technological developments till to date, Addit. Manuf. 19 (2018) 134–159, <http://dx.doi.org/10.1016/j.addma.2017.07.001>.
- [5] M.R. Rokni, S.R. Nutt, C.A. Widener, V.K. Champagne, R.H. Hrabe, Review of relationship between particle deformation, coating microstructure, and properties in high-pressure cold spray, J. Therm. Spray. Technol. (2017) 1–48, <http://dx.doi.org/10.1007/s11666-017-0575-0>.
- [6] M. Hassani-Gangaraj, D. Veysset, K.A. Nelson, C. Schuh, In-situ observations of single micro-particle impact bonding, Scr. Mater. (2017) 9–13, <http://dx.doi.org/10.1016/j.scriptamat.2017.09.042> in press.
- [7] F. Meng, S. Yue, J. Song, Quantitative prediction of critical velocity and deposition efficiency in cold-spray: a finite-element study, Scr. Mater. 107 (2015) 83–87, <http://dx.doi.org/10.1016/j.scriptamat.2015.05.026>.
- [8] H. Assadi, F. Gärtner, T. Stoltenhoff, H. Kreye, Bonding mechanism in cold gas spraying, Acta Mater. 51 (2003) 4379–4394, [http://dx.doi.org/10.1016/S1359-6454\(03\)00274-X](http://dx.doi.org/10.1016/S1359-6454(03)00274-X).
- [9] F.F. Raletz, M. Vardelle, G. Ezoo, Critical particle velocity under cold spray conditions, Surf. Coatings Technol. 201 (2006) 1942–1947, <http://dx.doi.org/10.1016/j.surfcoat.2006.04.061>.
- [10] M. Hassani-Gangaraj, D. Veysset, K.A. Nelson, C.A. Schuh, Melting can hinder impact-induced adhesion, Phys. Rev. Lett. (2017) 1–5, <http://dx.doi.org/10.1103/PhysRevLett.119.175701> in press.
- [11] M. Gruijicic, C.L.C. Zhao, W.S.W. DeRosset, D. Helfritch, Adiabatic shear instability based mechanism for particles/substrate bonding in the cold-gas dynamic-spray process, Mater. Des. 25 (2004) 681–688, <http://dx.doi.org/10.1016/j.matdes.2004.03.008>.
- [12] H. Assadi, T. Schmidt, H. Richter, J.O. Kliemann, K. Binder, F. Gärtner, et al., On parameter selection in cold spraying, J. Therm. Spray. Technol. 20 (2011) 1161–1176, <http://dx.doi.org/10.1007/s11666-011-9662-9>.
- [13] T. Schmidt, F. Gärtner, H. Assadi, H. Kreye, Development of a generalized parameter window for cold spray deposition, Acta Mater. 54 (2006) 729–742, <http://dx.doi.org/10.1016/j.actamat.2005.10.005>.
- [14] G. Bae, S. Kumar, S. Yoon, K. Kang, H. Na, H.J. Kim, et al., Bonding features and associated mechanisms in kinetic sprayed titanium coatings, Acta Mater. 57 (2009) 5654–5666, <http://dx.doi.org/10.1016/j.actamat.2009.07.061>.
- [15] S. Yin, X. Wang, X. Suo, H. Liao, Z. Guo, W. Li, et al., Deposition behavior of thermally softened copper particles in cold spraying, Acta Mater. 61 (2013) 5105–5118, <http://dx.doi.org/10.1016/j.actamat.2013.04.041>.
- [16] S. Yin, M. Meyer, W. Li, H. Liao, R. Lupoi, Gas flow, particle acceleration, and heat transfer in cold spray: a review, J. Therm. Spray Technol. 25 (2016) 1–23, <http://dx.doi.org/10.1007/s11666-016-0406-8>.
- [17] J. Villafuerte, Current and future applications of cold spray technology, Met. Finish. 108 (2010) 37–39 <http://www.scopus.com/inward/record.url?eid=2-s2.0-76949092433&partnerID=40&md5=86b2291131b8deebbd875d7db978580>.
- [18] A. Kashirin, O. Klyuev, T. Buzdygar, A. Shkodkin, Modern applications of the low pressure cold spray, Proc. 2011 Int. Therm. Spray Conf., Hamburg, (2011).
- [19] V. Champagne, D. Helfritch, The unique abilities of cold spray deposition, Int. Mater. Rev. 6608 (2016) 1–19, <http://dx.doi.org/10.1080/09506608.2016.1194948>.
- [20] A.M. Vilardell, N. Cinca, A. Concusell, S. Dosta, I.G. Cano, J.M. Guilemany, Cold spray as an emerging technology for biocompatible and antibacterial coatings: state of art, J. Mater. Sci. (2015) 4441–4462, <http://dx.doi.org/10.1007/s10853-015-9013-1>.
- [21] V.K. Champagne, D.J. Helfritch, Mainstreaming cold spray – push for applications, Surf. Eng. 30 (2014) 396–403, <http://dx.doi.org/10.1179/1743294414Y.0000000277>.
- [22] W. Li, K. Yang, S. Yin, X. Yang, Y. Xu, R. Lupoi, Solid-state additive manufacturing and repairing by cold spraying: a review, J. Mater. Sci. Technol. (2017) 1–18, <http://dx.doi.org/10.1016/j.jmst.2017.09.015>.
- [23] S. Yin, B. Aldwell, R. Lupoi, Cold Spray Additive Manufacture and Component Restoration, (2018), pp. 195–224.
- [24] D. Herzog, V. Seyda, E. Wycisk, C. Emmelmann, Additive manufacturing of metals, Acta Mater. 117 (2016) 371–392, <http://dx.doi.org/10.1016/j.actamat.2016.07.019>.
- [25] T. Debroy, H.L. Wei, J.S. Zuback, T. Mukherjee, J.W. Elmer, J.O. Milewski, et al., Additive manufacturing of metallic components – process, structure and properties, Prog. Mater. Sci. 92 (2017) 112–224, <http://dx.doi.org/10.1016/j.jpmatsci.2017.10.001>.
- [26] T. Lead, C. Boston, Cold Spray Metallization Technology Focus Area Status Fred Lancaster NAVAIR Cold Spray, (2017).
- [27] R. Huang, H. Fukanuma, Study of the influence of particle velocity on adhesive strength of cold spray deposits, J. Therm. Spray Technol. 21 (2012) 541–549, <http://dx.doi.org/10.1007/s11666-011-9707-0>.
- [28] D. Goldbaum, R.R. Chromik, S. Yue, E. Irisson, J.G. Legoux, Mechanical property mapping of cold sprayed Ti splats and coatings, J. Therm. Spray Technol. 20 (2011) 486–496, <http://dx.doi.org/10.1007/s11666-010-9546-4>.
- [29] K. Binder, J. Gottschalk, M. Kollenda, F. Gärtner, T. Klassen, Influence of impact angle and gas temperature on mechanical properties of titanium cold spray deposits, J. Therm. Spray Technol. 20 (2011) 234–242, <http://dx.doi.org/10.1007/s11666-010-9557-1>.
- [30] D. Goldbaum, J.M. Shockley, R.R. Chromik, A. Rezaeian, S. Yue, J.G. Legoux, et al., The effect of deposition conditions on adhesion strength of Ti and Ti6Al4V cold spray splats, J. Therm. Spray Technol. 21 (2012) 288–303, <http://dx.doi.org/10.1007/s11666-011-9720-3>.
- [31] V. Luzin, K. Spencer, M.X. Zhang, Residual stress and thermo-mechanical properties of cold spray metal coatings, Acta Mater. 59 (2011) 1259–1270, <http://dx.doi.org/10.1016/j.actamat.2010.10.058>.
- [32] G. Shayegan, H. Mahmoudi, R. Ghelichi, J. Villafuerte, J. Wang, M. Guagliano, et al., Residual stress induced by cold spray coating of magnesium AZ31B extrusion, Mater. Des. 60 (2014) 72–84, <http://dx.doi.org/10.1016/j.matdes.2014.03.054>.
- [33] P. Cavaliere, A. Silvello, Processing conditions affecting residual stresses and fatigue properties of cold spray deposits, Int. J. Adv. Manuf. Technol. 81 (2015) 1857–1862, <http://dx.doi.org/10.1007/s00170-015-7365-y>.

- [34] L. Venkatesh, N.M. Chavan, G. Sundararajan, The influence of powder particle velocity and microstructure on the properties of cold sprayed copper coatings, *J. Therm. Spray Technol.* 20 (2011) 1009–1021, <http://dx.doi.org/10.1007/s11666-011-9614-4>.
- [35] R. Ghelichi, S. Bagherifard, D. Macdonald, I. Fernandez-Pariente, B. Jodoin, M. Guagliano, Experimental and numerical study of residual stress evolution in cold spray coating, *Appl. Surf. Sci.* 288 (2014) 26–33, <http://dx.doi.org/10.1016/j.apsusc.2013.09.074>.
- [36] K. Petráčková, J. Kondás, M. Guagliano, Mechanical performance of cold-sprayed A357 aluminum alloy coatings for repair and additive manufacturing, *J. Therm. Spray Technol.* (2017) 1–10, <http://dx.doi.org/10.1007/s11666-017-0643-5>.
- [37] P.D. Eason, S.C. Kennett, T.J. Eden, I. Krull, B. Kowalski, J.L. Jones, In situ observation of microstrain relief in cold-sprayed bulk copper during thermal annealing, *Scr. Mater.* 67 (2012) 791–794, <http://dx.doi.org/10.1016/j.scriptamat.2012.07.029>.
- [38] M. Meyer, S. Yin, K.A. Medonnell, O. Stier, R. Lupoi, Feed rate effect on particulate acceleration in cold spray under low stagnation pressure conditions, *Surf. Coatings Technol.* (2016) 237–245, <http://dx.doi.org/10.1016/j.surfcoat.2016.07.017> in review.
- [39] M. Meyer, S. Yin, R. Lupoi, particle in-flight velocity and dispersion measurements at increasing particle feed rates in cold spray, *J. Therm. Spray Technol.* 26 (2017) 60–70, <http://dx.doi.org/10.1007/s11666-016-0496-3>.
- [40] O.C. Ozdemir, C.A. Widener, M.J. Carter, K.W. Johnson, Predicting the effects of powder feeding rates on particle impact conditions and cold spray deposited coatings, *J. Therm. Spray Technol.* (2017), <http://dx.doi.org/10.1007/s11666-017-0611-0>.
- [41] K. Taylor, B. Jodoin, J. Karov, Particle loading effect in cold spray, *J. Therm. Spray Technol.* 15 (2006) 273–279, <http://dx.doi.org/10.1361/105996306X108237>.
- [42] J. Pattison, S. Celotto, R. Morgan, M. Bray, W. O'Neill, Cold gas dynamic manufacturing: a non-thermal approach to freeform fabrication, *Int. J. Mach. Tools Manuf.* 47 (2007) 627–634, <http://dx.doi.org/10.1016/j.ijmachtools.2006.05.001>.
- [43] A. Sova, S. Grigoriev, A. Okunkova, I. Smurov, Potential of cold gas dynamic spray as additive manufacturing technology, *Int. J. Adv. Manuf. Technol.* 69 (2013) 2269–2278, <http://dx.doi.org/10.1007/s00170-013-5166-8>.
- [44] D. Fang, S. Deng, H. Liao, C. Coddet, The effect of robot kinematics on the coating thickness uniformity, *J. Therm. Spray Technol.* 19 (2010) 796–804, <http://dx.doi.org/10.1007/s11666-010-9470-7>.
- [45] S. Deng, H. Liang, Z. Cai, H. Liao, G. Montavon, Kinematic optimization of robot trajectories for thermal spray coating application, *J. Therm. Spray Technol.* 23 (2014) 1382–1389, <http://dx.doi.org/10.1007/s11666-014-0137-7>.
- [46] D. Kotoban, S. Grigoriev, A. Okunkova, A. Sova, Influence of a shape of single track on deposition efficiency of 316L stainless steel powder in cold spray, *Surf. Coatings Technol.* 309 (2016) 2–9, <http://dx.doi.org/10.1016/j.surfcoat.2016.10.052>.
- [47] A.W.-Y.Y. Tan, W. Sun, Y.P. Phang, M. Dai, I. Marinescu, Z. Dong, et al., Effects of traverse scanning speed of spray nozzle on the microstructure and mechanical properties of cold-sprayed Ti6Al4V coatings, *J. Therm. Spray Technol.* 26 (2017) 1484–1497, <http://dx.doi.org/10.1007/s11666-017-0619-5>.
- [48] C. Chen, Y. Xie, C. Verdy, H. Liao, S. Deng, Modelling of coating thickness distribution and its application in offline programming software, *Surf. Coatings Technol.* (2016), <http://dx.doi.org/10.1016/j.surfcoat.2016.10.044>.
- [49] V.K. Champagne, D.J. Helfritch, S.P.G. Dinavahi, P.F. Leyman, Theoretical and experimental particle velocity in cold spray, *J. Therm. Spray Technol.* 20 (2011) 425–431, <http://dx.doi.org/10.1007/s11666-010-9530-z>.
- [50] H. Tabbara, S. Gu, D.G. McCartney, T.S. Price, P.H. Shipway, Study on process optimization of cold gas spraying, *J. Therm. Spray Technol.* 20 (2011) 608–620, <http://dx.doi.org/10.1007/s11666-010-9564-2>.
- [51] S. Yin, Q. Liu, H. Liao, X. Wang, Effect of injection pressure on particle acceleration, dispersion and deposition in cold spray, *Comput. Mater. Sci.* 90 (2014) 7–15, <http://dx.doi.org/10.1016/j.commatsci.2014.03.055>.
- [52] S. Rech, A. Trentin, S. Vezzù, E. Vedelago, J.-G. Legoux, E. Irissou, Different cold spray deposition strategies: single- and multi-layers to repair aluminium alloy components, *J. Therm. Spray Technol.* 6061 (2014) 1237–1250, <http://dx.doi.org/10.1007/s11666-014-0141-y>.
- [53] A. Moridi, S.M. Hassani Gangaraj, S. Vezzu, M. Guagliano, Number of passes and thickness effect on mechanical characteristics of cold spray coating, *Procedia Eng.* 74 (2014) 449–459, <http://dx.doi.org/10.1016/j.proeng.2014.06.296>.
- [54] S. Yin, X. Suo, Y. Xie, W. Li, R. Lupoi, H. Liao, Effect of substrate temperature on interfacial bonding for cold spray of Ni onto Cu, *J. Mater. Sci.* 50 (2015) 7448–7457, <http://dx.doi.org/10.1007/s10853-015-9304-6>.
- [55] A. Candel, R. Gadew, Trajectory generation and coupled numerical simulation for thermal spraying applications on complex geometries, *J. Therm. Spray Technol.* 18 (2009) 981–987, <http://dx.doi.org/10.1007/s11666-009-9338-x>.
- [56] Z. Cai, S. Deng, H. Liao, C. Zeng, G. Montavon, The effect of spray distance and scanning step on the coating thickness uniformity in cold spray process, *J. Therm. Spray Technol.* 23 (2014) 354–362, <http://dx.doi.org/10.1007/s11666-013-0002-0>.
- [57] S. Yin, X. Suo, H. Liao, Z. Guo, X. Wang, Significant influence of carrier gas temperature during the cold spray process, *Surf. Eng.* 30 (2014) 443–450, <http://dx.doi.org/10.1179/1743294414y.0000000276>.
- [58] J. Pattison, S. Celotto, A. Khan, W. O'Neill, Standoff distance and bow shock phenomena in the cold spray process, *Surf. Coatings Technol.* 202 (2008) 1443–1454, <http://dx.doi.org/10.1016/j.surfcoat.2007.06.065>.
- [59] W.Y. Li, C. Zhang, X.P. Guo, G. Zhang, H.L. Liao, C.J. Li, et al., Effect of standoff distance on coating deposition characteristics in cold spraying, *Mater. Des.* 29 (2008) 297–304, <http://dx.doi.org/10.1016/j.matdes.2007.02.005>.
- [60] R. Singh, K.H. Rauwald, E. Wessel, G. Mauer, S. Schruefer, A. Barth, et al., Effects of substrate roughness and spray-angle on deposition behavior of cold-sprayed Inconel 718, *Surf. Coatings Technol.* 319 (2017) 249–259, <http://dx.doi.org/10.1016/j.surfcoat.2017.03.072>.
- [61] J. Won, G. Bae, K. Kang, C. Lee, S.J. Kim, K.A. Lee, et al., Bonding, reactivity, and mechanical properties of the kinetic-sprayed deposition of Al for a thermally activated reactive Cu liner, *J. Therm. Spray Technol.* 23 (2014) 818–826, <http://dx.doi.org/10.1007/s11666-014-0088-z>.
- [62] N.B. Maledi, O.P. Oladijo, I. Botef, T.P. Ntsoane, A. Madiseng, L. Moloisane, Influence of cold spray parameters on the microstructures and residual stress of Zn coatings sprayed on mild steel, *Surf. Coatings Technol.* 318 (2017) 106–113, <http://dx.doi.org/10.1016/j.surfcoat.2017.03.062>.
- [63] P. Cavaliere, A. Silvello, N. Cinca, H. Canales, S. Dosta, I. Garcia Cano, et al., Microstructural and fatigue behavior of cold sprayed Ni-based superalloys coatings, *Surf. Coatings Technol.* 324 (2017) 390–402, <http://dx.doi.org/10.1016/j.surfcoat.2017.06.006>.
- [64] W.Y. Li, S. Yin, X.F. Wang, Numerical investigations of the effect of oblique impact on particle deformation in cold spraying by the SPH method, *Appl. Surf. Sci.* 256 (2010) 3725–3734, <http://dx.doi.org/10.1016/j.apsusc.2010.01.014>.
- [65] C. Chen, Y. Xie, S. Yin, M.-P. Planche, S. Deng, R. Lupoi, et al., Evaluation of the interfacial bonding between particles and substrate in angular cold spray, *Mater. Lett.* 173 (2016) 76–79, <http://dx.doi.org/10.1016/j.matlet.2016.03.036>.
- [66] S. Yin, X. Suo, J. Su, Z. Guo, H. Liao, X. Wang, Effects of substrate hardness and spray angle on the deposition behavior of Cold-sprayed Ti particles, *J. Therm. Spray Technol.* 23 (2013) 76–83, <http://dx.doi.org/10.1007/s11666-013-0039-0>.
- [67] D.L. Gilmore, R.C. Dykhuizen, R.A. Neiser, T.J. Roemer, M.F. Smith, Particle velocity and deposition efficiency in the cold spray process, *J. Therm. Spray Technol.* 8 (1999) 576–582, <http://dx.doi.org/10.1361/105996399770350278>.
- [68] C.-J. Li, W.-Y. Li, H. Liao, Examination of the critical velocity for deposition of particles in cold spraying, *J. Therm. Spray Technol.* 15 (2006) 212–222, <http://dx.doi.org/10.1361/105996306X1080939>.
- [69] C.J. Li, W.Y. Li, Y.Y. Wang, G.J. Yang, H. Fukanuma, A theoretical model for prediction of deposition efficiency in cold spraying, *Thin Solid Films.* 489 (2005) 79–85, <http://dx.doi.org/10.1016/j.tsf.2005.05.002>.
- [70] X.T. Luo, Y.J. Li, C.J.C.X. Li, G.J. Yang, C.J.C.X. Li, Effect of spray conditions on deposition behavior and microstructure of cold sprayed Ni coatings sprayed with a porous electrolytic Ni powder, *Surf. Coatings Technol.* 289 (2016) 85–93, <http://dx.doi.org/10.1016/j.surfcoat.2016.01.058>.
- [71] M.E. Lynch, W. Gu, T. El-Wardany, A. Hsu, D. Viens, A. Nardi, et al., Design and topology/shape structural optimisation for additively manufactured cold sprayed components, *Virtual Phys. Prototyp.* 8 (2013) 213–231, <http://dx.doi.org/10.1080/17452759.2013.837629>.
- [72] O. Stier, *Economics of cold spray – fundamental cost analysis*, CSAT Workshop, Worcester, USA, 2012.
- [73] O. Stier, Fundamental cost analysis of cold spray, *J. Therm. Spray Technol.* 23 (2013) 131–139, <http://dx.doi.org/10.1007/s11666-013-9972-1>.
- [74] C. Chen, S. Gojon, Y. Xie, S. Yin, C. Verdy, Z. Ren, et al., A novel spiral trajectory for damage component recovery with cold spray, *Surf. Coatings Technol.* (2016), <http://dx.doi.org/10.1016/j.surfcoat.2016.10.096>.
- [75] T. Suhonen, T. Varis, S. Dosta, M. Torrell, J.M. Guilemany, Residual stress development in cold sprayed Al, Cu and Ti coatings, *Acta Mater.* 61 (2013) 6329–6337, <http://dx.doi.org/10.1016/j.actamat.2013.06.033>.
- [76] P. Coddet, C. Verdy, C. Coddet, F. Debray, Mechanical properties of Cu-0.1Ag alloys deposited by cold spray with various powder feed rate and heat treatment, *J. Therm. Spray Technol.* 24 (2014) 119–125, <http://dx.doi.org/10.1007/s11666-014-0159-1>.
- [77] P. Coddet, C. Verdy, C. Coddet, F. Lecouturier, F. Debray, Comparison of the properties of cold-sprayed Cu-0.5Cr-0.05Zr alloys after various heat treatments versus forged and vacuum plasma-sprayed alloys, *J. Therm. Spray Technol.* 23 (2014) 486–491, <http://dx.doi.org/10.1007/s11666-013-0028-3>.
- [78] S. Bagherifard, G. Roscioli, M.V. Zuccoli, M. Hadi, G. D'Elia, A.G. Demir, et al., Cold spray deposition of freestanding inconel samples and comparative analysis with selective laser melting, *J. Therm. Spray Technol.* 26 (2017) 1517–1526, <http://dx.doi.org/10.1007/s11666-017-0572-3>.
- [79] R.N. Raolison, E. Aubignat, M.P. Planche, S. Costil, C. Langlade, H. Liao, Low pressure cold spraying under 6 bar pressure deposition: exploration of high deposition efficiency solutions using a mathematical modelling, *Surf. Coatings Technol.* 302 (2016) 47–55, <http://dx.doi.org/10.1016/j.surfcoat.2016.05.068>.
- [80] X. Meng, J. Zhang, J. Zhao, Y. Liang, Y. Zhang, Influence of gas temperature on microstructure and properties of cold spray 304SS coating, *J. Mater. Sci. Technol.* 27 (2011) 809–815, [http://dx.doi.org/10.1016/S1005-0302\(11\)60147-3](http://dx.doi.org/10.1016/S1005-0302(11)60147-3).
- [81] R. Huang, M. Sone, W. Ma, H. Fukanuma, The effects of heat treatment on the mechanical properties of cold-sprayed coatings, *Surf. Coatings Technol.* 261 (2015) 278–288, <http://dx.doi.org/10.1016/j.surfcoat.2014.11.017>.
- [82] K. Ito, K. Ogawa, Effects of spark-plasma sintering treatment on cold-sprayed copper coatings, *J. Therm. Spray Technol.* 23 (2014) 104–113, <http://dx.doi.org/10.1007/s11666-013-0047-0>.
- [83] F. Gärtner, T. Stoltenhoff, J. Voyer, H. Kreye, S. Riekehr, M. Koçak, Mechanical properties of cold-sprayed and thermally sprayed copper coatings, *Surf. Coatings Technol.* 200 (2006) 6770–6782, <http://dx.doi.org/10.1016/j.surfcoat.2005.10.007>.
- [84] T. Stoltenhoff, C. Borchers, F. Gärtner, H. Kreye, Microstructures and key properties of cold-sprayed and thermally sprayed copper coatings, *Surf. Coatings Technol.* 200 (2006) 4947–4960, <http://dx.doi.org/10.1016/j.surfcoat.2005.10.007>.

- [85] N. Kang, P. Coddet, H. Liao, C. Coddet, Cold gas dynamic spraying of a novel micro-alloyed copper: microstructure, mechanical properties, *J. Alloys Compd.* 686 (2016) 399–406, <http://dx.doi.org/10.1016/j.jallcom.2016.06.037>.
- [86] C. Borchers, F. Gärtnner, T. Stoltenhoff, H. Kreye, Formation of persistent dislocation loops by ultra-high strain-rate deformation during cold spraying, *Acta Mater.* 53 (2005) 2991–3000, <http://dx.doi.org/10.1016/j.actamat.2005.02.048>.
- [87] P. Sudharshan Phani, D. Srinivasa Rao, S.V. Joshi, G. Sundararajan, Effect of process parameters and heat treatments on properties of cold sprayed copper coatings, *J. Therm. Spray Technol.* 16 (2007) 425–434, <http://dx.doi.org/10.1007/s11666-007-9048-1>.
- [88] G. Sundararajan, N.M. Chavan, G. Sivakumar, P. Sudharshan Phani, Evaluation of parameters for assessment of inter-splat bond strength in cold-sprayed coatings, *J. Therm. Spray Technol.* 19 (2010) 1255–1266, <http://dx.doi.org/10.1007/s11666-010-9527-7>.
- [89] G. Sundararajan, N.M. Chavan, S. Kumar, The elastic modulus of cold spray coatings: influence of inter-splat boundary cracking, *J. Therm. Spray Technol.* 22 (2013) 1348–1357, <http://dx.doi.org/10.1007/s11666-013-0034-5>.
- [90] D. Seo, K. Ogawa, K. Sakaguchi, N. Miyamoto, Y. Suzuki, Parameter study influencing thermal conductivity of annealed pure copper coatings deposited by selective cold spray processes, *Surf. Coatings Technol.* 206 (2012) 2316–2324, <http://dx.doi.org/10.1016/j.surcoat.2011.10.010>.
- [91] H. Koivuluoto, A. Coleman, K. Murray, M. Kearns, P. Vuoristo, High pressure cold sprayed (HPCS) and low pressure cold sprayed (LPCS) coatings prepared from OFHC Cu feedstock: overview from powder characteristics to coating properties, *J. Therm. Spray Technol.* 21 (2012) 1065–1075, <http://dx.doi.org/10.1007/s11666-012-9790-x>.
- [92] M. Winnicki, A. Małachowska, A. Baszczuk, M. Rutkowska-Gorczyca, D. Kukla, M. Lachowicz, et al., Corrosion protection and electrical conductivity of copper coatings deposited by low-pressure cold spraying, *Surf. Coatings Technol.* 318 (2017) 90–98, <http://dx.doi.org/10.1016/j.surcoat.2016.12.101>.
- [93] S. Yin, L. Rocco, Microstructure and mechanical anisotropy of additively manufactured cold spray copper deposits, *Mater. Sci. Eng. A.* (2018).
- [94] W.-Y. Li, C.-J. Li, H. Liao, Effect of annealing treatment on the microstructure and properties of cold-sprayed Cu coating, *J. Therm. Spray Technol.* 15 (2006) 206–211, <http://dx.doi.org/10.1361/105996306X108066>.
- [95] H. Yu, A.K. Tieu, C. Lu, X. Liu, M. Liu, A. Godbole, et al., A new insight into ductile fracture of ultrafine-grained Al-Mg alloys, *Sci. Rep.* 5 (2015) 9568, <http://dx.doi.org/10.1038/srep09568>.
- [96] N. Kamikawa, X. Huang, N. Tsuji, N. Hansen, Strengthening mechanisms in nanostructured high-purity aluminium deformed to high strain and annealed, *Acta Mater.* 57 (2009) 4198–4208, <http://dx.doi.org/10.1016/j.actamat.2009.05.017>.
- [97] J.C. Lee, H.J. Kang, W.S. Chu, S.H. Ahn, Repair of damaged mold surface by cold-spray method, *CIRP Ann.- Manuf. Technol.* 56 (2007) 577–580, <http://dx.doi.org/10.1016/j.cirp.2007.05.138>.
- [98] B. Aldwell, E. Kelly, R. Wall, A. Amaldi, G.E. O'Donnell, R. Lupoi, Machinability of Al 6061 deposited with cold spray additive manufacturing, *J. Therm. Spray Technol.* 26 (2017) 1573–1584, <http://dx.doi.org/10.1007/s11666-017-0586-x>.
- [99] A. Sova, C. Courbon, F. Valiorgue, J. Rech, P. Bertrand, Effect of turning and ball burnishing on the microstructure and residual stress distribution in stainless steel cold spray deposits, *J. Therm. Spray Technol.* 26 (2017) 1922–1934, <http://dx.doi.org/10.1007/s11666-017-0655-1>.
- [100] S. Yin, X. Wang, W. Li, H. Liao, H. Jie, Deformation behavior of the oxide film on the surface of cold sprayed powder particle, *Appl. Surf. Sci.* 259 (2012) 294–300, <http://dx.doi.org/10.1016/j.apsusc.2012.07.036>.
- [101] M. Czampa, S. Markos, T. Szalay, Improvement of drilling possibilities for machining powder metallurgy materials, *Procedia CIRP.* 7 (2013) 288–293, <http://dx.doi.org/10.1016/j.procir.2013.05.049>.
- [102] A. Bordin, A. Ghiotti, S. Bruschi, L. Facchini, F. Buccianti, Machinability characteristics of wrought and EBM CoCrMo alloys, *Procedia CIRP.* 14 (2014) 89–94, <http://dx.doi.org/10.1016/j.procir.2014.03.082>.
- [103] M.S.A. Aziz, T. Ueda, T. Furumoto, S. Abe, A. Hosokawa, A. Yassin, Study on machinability of laser sintered materials fabricated by layered manufacturing system: influence of different hardness of sintered materials, *Procedia CIRP.* 4 (2012) 79–83, <http://dx.doi.org/10.1016/j.procir.2012.10.015>.
- [104] F. Montecuccchi, N. Grossi, H. Takagi, A. Scippa, H. Sasahara, G. Campatelli, Cutting forces analysis in additive manufactured AISI H13 alloy, *Procedia CIRP* 46 (2016) 476–479, <http://dx.doi.org/10.1016/j.procir.2016.04.034>.
- [105] O.R. Tutunea-Fatan, Ma. Fakhri, E.V. Bordatchev, Porosity and cutting forces: from macroscale to microscale machining correlations, *Proc. Inst. Mech. Eng. Part B: J. Eng. Manuf.* 225 (2011) 619–630, <http://dx.doi.org/10.1177/2041297510394057>.
- [106] M. Abolghasemi Fakhri, E.V. Bordatchev, O.R. Tutunea-Fatan, An image-based methodology to establish correlations between porosity and cutting force in micromilling of porous titanium foams, *Int. J. Adv. Manuf. Technol.* 60 (2012) 841–851, <http://dx.doi.org/10.1007/s00170-011-3647-1>.
- [107] G. Lu, G.Q. Lu, Z.M. Xiao, Mechanical properties of porous materials, *J. Porous Mater.* 6 (1999) 359–368, <http://dx.doi.org/10.1023/A:1009669730778>.
- [108] M. Ramulu, P.N. Rao, H. Kao, Drilling of (Al203)p/6061 metal matrix composites, *J. Mater. Process. Technol.* 124 (2002) 244–254, [http://dx.doi.org/10.1016/S0924-0136\(02\)00176-0](http://dx.doi.org/10.1016/S0924-0136(02)00176-0).
- [109] D. MacDonald, R. Fernández, F. Delloro, B. Jodoin, Cold spraying of armstrong process titanium powder for additive manufacturing, *J. Therm. Spray Technol.* (2016), <http://dx.doi.org/10.1007/s11666-016-0489-2>.
- [110] M. Abreeza, I. Yuji, O. Kazuhiro, Computational simulation for cold sprayed deposition, *Sendai, Japan* (2011).
- [111] B. Barnett, M. Trexler, V. Champagne, Cold sprayed refractory metals for chrome reduction in gun barrel liners, *Int. J. Refract. Met. Hard Mater.* 53 (2015) 139–143, <http://dx.doi.org/10.1016/j.ijrmhm.2015.07.007>.
- [112] H.J. Choi, M. Lee, J.Y. Lee, Application of a cold spray technique to the fabrication of a copper canister for the geological disposal of CANDU spent fuels, *Nucl. Eng. Des.* 240 (2010) 2714–2720, <http://dx.doi.org/10.1016/j.nucengdes.2010.06.038>.
- [113] S. Kumar, N.M. Chavan, *Cold Spray Coating Technology: Activities at ARCI, Hyderabad, India*, (2011).
- [114] H. Chad, *CSIRO Titanium Technologies and Additive Manufacturing*, (2014).
- [115] P. Richter, *New Value Chain for Advanced Coatings by Using Cold Spray*, (2014) Athens, Greece.
- [116] C. May, S. Marx, A. Paul, *Selected R&D Results and Industrial Applications*, Freiberg, Germany, 2013.
- [117] A. Sova, A. Okunkova, S. Grigoriev, I. Smurov, Velocity of the particles accelerated by a cold spray micronozzle: experimental measurements and numerical simulation, *J. Therm. Spray Technol.* 22 (2013) 75–80, <http://dx.doi.org/10.1007/s11666-012-9846-y>.
- [118] T. Briefing, *Metal coated particles and defense applications*, CSAT Workshop, Worcester, USA, 2013.
- [119] J. Villafuerte, *Using Cold Spray to Add Features to Components*, (2015).
- [120] Y. Cormier, P. Dupuis, A. Farjam, A. Corbeil, B. Jodoin, Additive manufacturing of pyramidal pin fins: height and fin density effects under forced convection, *Int. J. Heat Mass Transf.* 75 (2014) 235–244, <http://dx.doi.org/10.1016/j.ijheatmasstransfer.2014.03.053>.
- [121] Y. Cormier, P. Dupuis, B. Jodoin, A. Corbeil, Pyramidal Fin arrays performance using streamwise anisotropic materials by cold spray additive manufacturing, *J. Therm. Spray Technol.* 25 (2016) 170–182, <http://dx.doi.org/10.1007/s11666-015-0267-6>.
- [122] P. Dupuis, Y. Cormier, M. Fenech, A. Corbeil, B. Jodoin, Flow structure identification and analysis in fin arrays produced by cold spray additive manufacturing, *Int. J. Heat Mass Transf.* 93 (2016) 301–313, <http://dx.doi.org/10.1016/j.ijheatmasstransfer.2015.10.019>.
- [123] P. Dupuis, Y. Cormier, M. Fenech, B. Jodoin, Heat transfer and flow structure characterization for pin fins produced by cold spray additive manufacturing, *Int. J. Heat Mass Transf.* 98 (2016) 650–661, <http://dx.doi.org/10.1016/j.ijheatmasstransfer.2016.03.069>.
- [124] Y. Cormier, P. Dupuis, B. Jodoin, A. Ghaei, Finite element analysis and failure mode characterization of pyramidal fin arrays produced by masked cold gas dynamic spray, *J. Therm. Spray Technol.* 24 (2015) 1549–1565, <http://dx.doi.org/10.1007/s11666-015-0317-0>.
- [125] A. Farjam, Y. Cormier, P. Dupuis, B. Jodoin, A. Corbeil, Influence of alumina addition to aluminum fins for compact heat exchangers produced by cold spray additive manufacturing, *J. Therm. Spray Technol.* 24 (2015) 1256–1268, <http://dx.doi.org/10.1007/s11666-015-0305-4>.
- [126] Y. Cormier, P. Dupuis, B. Jodoin, A. Corbeil, Net shape fins for compact heat exchanger produced by cold spray, *J. Therm. Spray Technol.* 22 (2013) 1210–1221, <http://dx.doi.org/10.1007/s11666-013-9968-x>.
- [127] Y. Cormier, P. Dupuis, B. Jodoin, A. Corbeil, Mechanical properties of cold gas dynamic-sprayed near-net-shaped Fin arrays, *J. Therm. Spray Technol.* 24 (2014) 476–488, <http://dx.doi.org/10.1007/s11666-014-0203-1>.
- [128] W. Birth, *Practical Cold Spray*, (2010).
- [129] B. Bierk, G. Mgr, G. Addison, B. Elmquist, *Repair technology development projects*, CSAT Workshop, Worcester, USA, 2011.
- [130] S. Yin, Y. Xie, X. Suo, H. Liao, X. Wang, Interfacial bonding features of Ni coating on Al substrate with different surface pretreatments in cold spray, *Mater. Lett.* 138 (2015) 143–147, <http://dx.doi.org/10.1016/j.matlet.2014.10.016>.
- [131] A. Nastic, M. Vijay, A. Tieu, S. Rahmati, B. Jodoin, Experimental and numerical study of the influence of substrate surface preparation on adhesion mechanisms of aluminum cold spray coatings on 300M steel substrates, *J. Therm. Spray Technol.* 26 (2017) 1461–1483, <http://dx.doi.org/10.1007/s11666-017-0602-1>.
- [132] W. Sun, A.W.Y. Tan, N.W. Khun, I. Marinescu, E. Liu, Effect of substrate surface condition on fatigue behavior of cold sprayed Ti6Al4V coatings, *Surf. Coatings Technol.* 320 (2017) 452–457, <http://dx.doi.org/10.1016/j.surcoat.2016.11.093>.
- [133] J. Schell, *Cold spray aerospace applications*, CSAT Workshop, Worcester, USA, 2016.
- [134] C. Howe, *Cold spray repair of the CH-47 accessory cover*, CSAT Workshop, Worcester, USA, 2014.
- [135] G. Kilchenstein, *Cold spray technologies used for repair*, JTEG Mon. Teleconference, (2014).
- [136] B. DeForce, T. Eden, J. Potter, V. Champagne, P. Leyman, D. Helfritch, Application of aluminum coatings for the corrosion protection of magnesium by cold spray, *Tri-Service Corros. Conf.* Denver, USA, 2007 <http://www.arl.psu.edu/documents/TriService-paper-BDeForcerev1.pdf>.
- [137] V.K. Champagne, D. Helfritch, P.F. Leyman, Magnesium repair by cold spray, *Plat. Surf. Finish.* 95 (2008) 19–28 <http://www.scopus.com/inward/record.url?eid=2-s2.0-70349786053&partnerID=40&md5=84aac69203b4e8a38e69574497338189>.
- [138] E. Security, T.C. Program, Cost and Performance Report Cold Spray for Repair of Magnesium, (2011) <http://www.dtic.mil/dtic/tr/fulltext/u2/a572962.pdf>.
- [139] P.F. Leyman, V.K. Champagne, Cold Spray Process Development for the Reclamation of the Apache Helicopter Mast Support, (2009) <http://www.dtic.mil/get-tr-doc/pdf?AD=ADA505530>.
- [140] C. Howe, *Cold spray qualification of T700 engine front frame*, CSAT Workshop, Worcester, USA, 2015.
- [141] C.A. Widener, M.J. Carter, O.C. Ozdemir, R.H. Hrabe, B. Hoiland, T.E. Stamey, et al., Application of high-pressure cold spray for an internal bore repair of a navy

- valve actuator, *J. Therm. Spray Technol.* 25 (2016) 193–201, <http://dx.doi.org/10.1007/s11666-015-0366-4>.
- [142] V.P. Lyalyakin, A.Y. Kostukov, V.A. Denisov, Special features of reconditioning the housing of a caterpillar diesel oil pump by gas-dynamic spraying, *Weld. Int.* 30 (2016) 68–70, <http://dx.doi.org/10.1080/09507116.2015.1030152>.
- [143] R.G. Maev, E. Strumban, V. Leshchinskiiy, D. Dzurinskiy, *Repair Applications of the LPCS Process*, CSAT Workshop, Worcester, USA, 2014.
- [144] B.S. D6-51343, *Thermal Spray Repair of Exterior Clad Aluminum*, USA, (2006).
- [145] R. Jones, L. Molent, S. Barter, N. Matthews, D. Tamboli, Supersonic particle deposition as a means for enhancing the structural integrity of aircraft structures, *Int. J. Fatigue* 68 (2014) 260–268, <http://dx.doi.org/10.1016/j.ijfatigue.2014.03.013>.
- [146] N. Matthews, R. Jones, G.C. Sih, Application of supersonic particle deposition to enhance the structural integrity of aircraft structures, *Sci. China Phys. Mech. Astron.* 57 (2014) 12–18, <http://dx.doi.org/10.1007/s11433-013-5367-z>.
- [147] R. Jones, N. Matthews, C.A. Rodopoulos, K. Cairns, S. Pitt, On the use of supersonic particle deposition to restore the structural integrity of damaged aircraft structures, *Int. J. Fatigue* 33 (2011) 1257–1267, <http://dx.doi.org/10.1016/j.ijfatigue.2011.03.013>.
- [148] M. Yandouzi, S. Gaydos, D. Guo, R. Ghelichi, B. Jodoin, Aircraft skin restoration and evaluation, *J. Therm. Spray Technol.* 23 (2014) 1281–1290, <http://dx.doi.org/10.1007/s11666-014-0130-1>.
- [149] P. Cavaliere, A. Silvello, Crack repair in aerospace aluminum alloy panels by cold spray, *J. Therm. Spray Technol.* 26 (2017) 661–670, <http://dx.doi.org/10.1007/s11666-017-0534-9>.
- [150] R. Jones, N. Matthews, J. Elston, K. Cairns, J. Baker, B. Wadsley, et al., Spd repairs to thin aluminium structures, *28th Int. Congr. Aeronaut. Sci.* (2012) 1–9.
- [151] T. Stoltenhoff, F. Zimmermann, P. Surface, T. GmbH, LOXPlate® Coatings for Aluminum Aerospace Components Exposed to High Dynamic Stresses, Ratingen, Germany (2012).